Advances in Colloid and Interface Science 216 (2015) 1–19

Contents lists available at ScienceDirect

Advances in Colloid and Interface Science

journal homepage: www.elsevier.com/locate/cis

Influence of surface roughness on dispersion forces

V.B. Svetovoy [a,*], G. Palasantzas [b]

[a] MESA+ Institute for Nanotechnology, University of Twente, PO 217, 7500 AE Enschede, The Netherlands
[b] Zernike Institute for Advanced Materials, University of Groningen, 9747 AG Groningen, The Netherlands

ARTICLE INFO

Available online 13 November 2014

Keywords:
Dispersion forces
Roughness
Nonadditivity
Contact
Adhesion

ABSTRACT

Surface roughness occurs in a wide variety of processes where it is both difficult to avoid and control. When two bodies are separated by a small distance the roughness starts to play an important role in the interaction between the bodies, their adhesion, and friction. Control of this short-distance interaction is crucial for micro and nanoelectromechanical devices, microfluidics, and for micro and nanotechnology. An important short-distance interaction is the dispersion forces, which are omnipresent due to their quantum origin. These forces between flat bodies can be described by the Lifshitz theory that takes into account the actual optical properties of interacting materials. However, this theory cannot describe rough bodies. The problem is complicated by the nonadditivity of the dispersion forces. Evaluation of the roughness effect becomes extremely difficult when roughness is comparable with the distance between bodies. In this paper we review the current state of the problem. Introduction for non-experts to physical origin of the dispersion forces is given in the paper. Critical experiments demonstrating the nonadditivity of the forces and strong influence of roughness on the interaction between bodies are reviewed. We also describe existing theoretical approaches to the problem. Recent advances in understanding the role of high asperities on the forces at distances close to contact are emphasized. Finally, some opinions about currently unsolved problems are also presented.

Contents

* Corresponding author.
E-mail address: v.svetovoy@utwente.nl (V.B. Svetovoy).

http://dx.doi.org/10.1016/j.cis.2014.11.001
0001-8686/

1. Introduction

Dispersion forces originate from quantum and thermal fluctuations of electric currents inside of interacting media and in the gap separating them [1–4]. Assuming flat surfaces, the forces increase as $d^{-\alpha}$ when distance d between bodies decreases. The exponent α is in between 3 and 4 depending on the distance. Conditionally the dispersion forces become dominant when the bodies are separated by the distances smaller than 100 nm. They play an important role in nanoscience and nanotechnology including micro and nanoelectromechanical devices [5–8]. The role of these forces is also essential in colloid and interface science [9–15]. In the latter case the interaction happens in a liquid medium, where in addition the electrostatic forces are involved. The dispersion forces are closely related to adhesion between bodies under dry conditions [16,17]. They define the adhesion energy as the force acting via the gap separating the bodies upon contact.

Historically different names are used for the forces, which we call here dispersion forces. At distances smaller than a few nanometers these forces are termed van der Waals forces [1]. At larger distances the same forces are called the retarded van der Waals forces or Casimir forces [2,19]. All these forces have the same physical origin related to fluctuating currents. To stress this point the general name Casimir–Lifshitz force is in use. Evgeny Lifshitz [3] was the first who recognized the common origin of the van der Waals and Casimir forces. He deduced the so-called Lifshitz formula [18], which is able to predict the force between two parallel plates separated by distance d using as input parameters the dielectric functions of interacting materials. Therefore the bodies within the Lifshitz theory are treated macroscopically. The minimal size in the Lifshitz theory is the size where the dielectric function is well defined (much larger than interatomic distances). The Lifshitz formula interpolates between the van der Waals force at small distances $d < 5$ nm and the pure Casimir force at $d > 1$ μm. Between parallel plates the first decreases as d^{-3} while the second one decreases as d^{-4} when the distance increases. In this paper to name all the forces having the same origin we use the general term dispersion forces proposed by London for molecules.

The dispersion forces are nonadditive. The force between two molecules depends on the position of a third molecule located nearby. A consequence is that the force between bodies of finite size cannot be calculated as pairwise summation of forces acting between separate molecules. This is an important point because it complicates the calculation of the force in many practical situations. Nonadditivity is often cited as a very specific property of the dispersion forces. However, the electrostatic force can also be nonadditive. The force between metallic sphere and plate cannot be calculated as the sum of forces between infinitesimal capacitors. The reason is that the charges redistribute in response to the field. A similar effect happens for the dispersion forces where polarization changes with the field.

One limitation of the Lifshitz formula is that the force is predicted explicitly only between parallel plates. It is not a principal restriction but rather a computational one related to nonadditivity. Only recently a closed-form expression for the sphere–plate interaction was presented [20,21]. Even for numerical calculations the problem was not an easy task but significant progress was made in the last decade and the force was evaluated for a number of geometrical configurations [22]. The same restriction exists for the Derjaguin–Landau–Verwey–Overbeek (DLVO) theory of colloidal stability [9,10] with an additional complication that includes electrostatic forces.

Nonadditivity makes the problem even more difficult if one would like to calculate the force between randomly rough bodies. All solids in nature or in laboratories are rough. The roughness can be characterized by two main parameters that are the root–mean–square (rms) roughness ξ (typical feature size). While w is much smaller than the distance between bodies d the roughness correction to the force can be calculated using the perturbation theory. The corresponding methods have been developed in relation to the precise measurements of the Casimir forces at distances larger than 100 nm [23–25]. However, when the force was measured at distances smaller than 100 nm, strong deviations from the predictions based on the perturbation theory were found [26] even for relatively small rms roughness $w \ll d$. As was explained later [27] this effect is due to significant deviations of the roughness statistics from the normal distribution for some materials.

The ultimate problem related to surface roughness is the evaluation of the force when the rms roughness is comparable with the distance between the bodies. At this moment the problem is not solved but it is clear that high peaks of the roughness profile play a principal role. For this reason the problem is closely related to the contact between two bodies. In principle the force can be calculated numerically, but practically it can be done only for a restricted area. Up to now the roughness effect was not tackled numerically. The important role of high peaks, which are rare statistical events, combined with numerical calculations and experimental data could give a strong push to understand the influence of roughness on dispersion forces.

The purpose of this paper is not only to review existing experimental and theoretical approaches to the roughness problem, which are still in their infancy, but also to give an introduction for non-experts to the methods used to calculate the dispersion forces in different practical situations. The paper is organized as follows. In Section 2 the physical origin of the dispersion forces is described and some helpful relations are presented. A review of experiments important for understanding of the roughness effect is presented in Section 3. Methods to describe rough surfaces and existing theoretical models for the force taking into account roughness effect are described in Section 4. Finally some conclusions and our vision of the problems that have to be solved are collected in the last chapter.

2. Dispersion forces

In this section we describe the main ideas and results of Lifshitz theory of dispersion forces. We try to present a clear physical picture and give the necessary equations in the form convenient for practical applications of the theory. This section can be considered as an introduction to the Lifshitz theory. Quite often it is not realized that so different physical phenomena as well-known van der Waals forces acting between macroscopic bodies separated by a few nanometers gap and rather

exotic Casimir forces related to the boundary conditions on perfectly reflecting mirrors separated by much larger distances are actually intimately related to each other. In terms of the Lifshitz theory both originate from fluctuating currents (or polarizations) in macroscopic bodies. The currents in one of the bodies give rise to the electromagnetic field interacting with the currents in the other body. If this distance is small, one can neglect the retardation effect and the resulting interaction reproduces the van der Waals forces. At larger distances the retardation becomes important and one can reproduce the Casimir forces.

2.1. Early representations

2.1.1. Van der Waals force

Van der Waals [28] introduced weak intermolecular forces to explain deviations from the ideal gas laws but the physical nature of these deviations stayed unclear. In 1930 London [1] showed how one can understand the long distance behavior of the forces using quantum mechanics. It was shown that the attractive forces appear from electrostatic interaction of temporary dipoles in atoms or molecules. If R is the distance between atoms, the interaction energy between them decays according to the power law: $V_{int} \sim R^{-6}$. The forces associated with this potential are called dispersion or induced London dipole–dipole forces.

Appearance of attractive forces between neutral atoms naturally leads to similar forces between any two macroscopic bodies separated by a distance d. The force between two macroscopic spheres was calculated for the first time by Hamaker [29] using pairwise summation of the van der Waals–London potential between atoms. Ironically this famous result happened to be incorrect. As became clear later the dispersion forces are nonadditive and the pairwise summation gives incorrect results in general. Nevertheless, at some conditions more precise calculations based on the Lifshitz theory showed that the Hamaker approach can be accepted as a convenient first approximation [30]. As a particular case, Hamaker found the van der Waals force (per unit area) between two parallel macroscopic slabs that had been derived earlier by de Boer [31] and this result is absolutely precise. As a function of distance d this force is

$$F_{vdW} = \frac{A_H}{6\pi d^3}, \tag{2.1}$$

where A_H is the so-called Hamaker constant [29] accounting for material properties of the slabs. Precise meaning of this constant and the range of distances where the formula (Eq. (2.1)) is applicable were clarified only after the development of the Lifshitz theory [3,4,18].

2.1.2. Casimir force

In 1948 Casimir [2] showed that two uncharged ideally reflecting mirrors parallel to each other and separated by a gap d will be mutually attracted. The force per unit area was found to be

$$F_C = \frac{\pi^2 \hbar c}{240 d^4}. \tag{2.2}$$

It is the famous Casimir formula. An exceptional feature of this formula is that the force depends only on the separation and fundamental constants; no electron charge enters the formula.

The attraction is attributed to quantum fluctuations of vacuum electromagnetic fields, which are different between the mirrors and outside of them due to the presence of ideally reflecting boundaries. Inside the cavity formed by the mirrors, only the modes that have nodes on the mirrors are allowed. Outside of the cavity all the modes can exist. In this situation the radiation pressure from the outside will be larger than that from the inside of the cavity. As the result the mirrors will attract each other. According to quantum mechanics each mode of the field with frequency ω has a zero-point energy $\hbar\omega/2$. Then the Casimir energy is the change in the zero-point energy of vacuum due to the presence of the boundaries.

Zero-point energy interpretation became so popular in the physics community that the other side of the problem is remembered mostly by experts in the field. Namely, in the same year of 1948, Casimir and Polder published a paper [19], where they took into account the retardation effect in the interaction between two induced dipoles. It was found that when the distance between atoms increases the interaction energy falls off with distance as $\sim 1/R^7$. It is faster than for the non-retarded van der Waals interaction ($\sim 1/R^6$). Casimir already realized [2] that the retarded interaction of dipoles has to give the force between macroscopic bodies, which behaves with the distance precisely as Eq. (2.2). However, the final clarification of this point was made by Lifshitz [3] who presented the van der Waals (Section 2.1.1) and Casimir (Section 2.1.2) forces as the limit cases of one and the same force at small and large distances, respectively.

2.2. Lifshitz theory

The most detailed theory of dispersion forces between macroscopic bodies was developed by Lifshitz in 1955. It was based on the Rytov's theory of fluctuating electromagnetic fields [32]. This theory is applicable, in principle, to any bodies, independent on their molecular constitution. It includes retardation effects automatically and the only restriction on the distance is that it must be much larger than the interatomic distance. An important feature of the theory is that it expresses the force via macroscopic dielectric functions of the bodies. An approach close to the original Lifshitz consideration is described briefly in [33]. Generalization of the theory to the case of liquid gap separating the bodies was developed by Dzyaloshinskii, Lifshitz, and Pitaevskii in 1961 [4] and became part of the textbook [18].

In general, the Lifshitz theory can be applied to bodies of arbitrary shape. However, in a closed form the expression for the dispersion forces can be given only for parallel plates separated by a gap. This is the most important restriction of the Lifshitz formula, which was recently overcome by the development of numerical procedure [34].

2.2.1. Physical ground

It is not possible to calculate the dispersion forces between macroscopic bodies starting from microscopic interaction between separate atoms. Pairwise summation would be valid only for rarefied bodies such as gases. In condensed bodies the atoms in the neighborhood cause an essential change in the properties of the electronic shells, and the presence of a medium between the interacting atoms affects the electromagnetic field through which the interaction is established [4]. Nonadditivity is often cited as a very specific property of the dispersion forces. However, the electrostatic interaction also demonstrates nonadditive properties when charges in the bodies are able to redistribute in response to the applied field.

Instead of a "microscopic" description of the problem one can use a macroscopic point of view, in which interacting bodies are treated as continuous media. This is possible when the bodies are separated by the distances large in comparison with interatomic distances.

The fundamental idea of the theory is that the interaction between the bodies is established through fluctuating electromagnetic fields. Such fields are always present inside and extend beyond material boundaries. A well-known example is thermal radiation but it has to be stressed that electromagnetic fluctuations persist even at zero temperature as zero-point quantum fluctuations. The source of these fluctuations is the electric polarization $\mathbf{P}(\omega, \mathbf{r})$ or equivalently the electric current density $\mathbf{J}(\omega, \mathbf{r}) = -i\omega\mathbf{P}(\omega, \mathbf{r})$, where we understand the physical values as Fourier transformed in time. The origin of fluctuating currents is easier to understand for metals. The density of quasi-free electrons in a metal fluctuates as the density of particles in any gas. If at a point $\mathbf{r}$ the density is smaller than the average value, there will be a current tending to increase the density at this point.

2.2.2. Fluctuation–dissipation theorem

According to the fluctuation dissipation theorem (FDT) [32,33,35] in thermal equilibrium the correlations of these fluctuating currents are related to the dissipation in the medium:

$$\left\langle J_\alpha(\omega,\mathbf{r})J^*_\beta(\omega',\mathbf{r}')\right\rangle = \omega\varepsilon''(\omega)\left(\frac{\hbar\omega}{2}+\frac{\hbar\omega}{e^{\hbar\omega/kT}-1}\right)\times\delta(\omega-\omega')\delta(\mathbf{r}-\mathbf{r}')\delta_{\alpha\beta}, \tag{2.3}$$

where $\alpha,\beta = x,y,z$ enumerate vector components, and the dissipation is proportional to the imaginary part of the dielectric function $\varepsilon''(\omega) = \mathrm{Im}\varepsilon(\omega)$. Due to FDT *the very existence of the dispersion forces is closely related to the dissipation in the materials of interacting bodies*. In Eq. (2.3) the contributions from the zero-point and thermal fluctuations are explicitly separated (the first and second terms in the brackets). Some additional information related to the application of FDT for calculating the dispersion forces including nonequilibrium situations can be found in [36–38].

Fluctuating currents are the sources of electromagnetic field. This field is described by the Maxwell equations. Solutions of these equations can be expressed via the Green functions. For example, the components of the electric field $E_\alpha(\omega,\mathbf{r})$ are

$$E_\alpha(\omega,\mathbf{r}) = \frac{i}{\omega}\int d\mathbf{r}' G_{\alpha\beta}(\omega,\mathbf{r},\mathbf{r}')J_\beta(\omega,\mathbf{r}'), \tag{2.4}$$

where $G_{\alpha\beta}$ are the components of the Green tensor. It is clear from Eq. (2.4) that the Green functions play the role of the response function in the linear-response theory [39].

Using the relation (2.4) together with the FDT (2.3) and making use of the general properties of the Green tensor we can find the correlation functions for the components of the electric field expressed via the Green functions:

$$\left\langle E_\alpha(\omega,\mathbf{r})E^*_\beta(\omega',\mathbf{r}')\right\rangle = 2\pi\hbar coth\left(\frac{\hbar\omega}{2kT}\right)\mathrm{Im}G_{\alpha\beta}(\omega,\mathbf{r},\mathbf{r}')\delta(\omega-\omega'). \tag{2.5}$$

The correlation functions of the magnetic field can be easily found by applying the Maxwell equations [18].

The Green tensor is the solution of the equation, which follows directly from the Maxwell equations:

$$\left[\partial_\alpha\partial_\beta-\delta_{\alpha\beta}\left(\nabla^2+\frac{\omega^2}{c^2}\varepsilon(\omega,\mathbf{r})\right)\right]G_{\alpha\gamma}(\omega,\mathbf{r},\mathbf{r}') = 4\pi\frac{\omega^2}{c^2}\delta_{\alpha\beta}\delta(\mathbf{r}-\mathbf{r}'). \tag{2.6}$$

Here $\varepsilon(\omega,\mathbf{r})$ is the nonhomogeneous dielectric function describing the interacting bodies. For example, if two bodies are interacting via a vacuum gap then $\varepsilon(\omega,\mathbf{r})$ is 1 within the gap, it is $\varepsilon_1(\omega)$ in the place filled with body 1 and is $\varepsilon_2(\omega)$ in the space occupied by body 2. Eq. (2.6) has to be solved with proper boundary conditions characterizing the field components at the interfaces [18]. In the sense of boundary conditions $G_{\alpha\beta}(\omega,\mathbf{r},\mathbf{r}')$ behaves as $E_\alpha(\omega,\mathbf{r})$.

The force acting on the body surface is the normal component of the Maxwell stress tensor. The averaged stress tensor can be expressed via the correlation functions (2.5) or finally via the Green functions of the system (2.6) at $\mathbf{r} = \mathbf{r}'$ where $\mathbf{r}$ approaches the surface from the side of the gap. In case of the gap filled with a liquid it is possible to do it due to equilibrium between absorption and emission [4]. This point was recently stressed again by Pitaevskii [40].

2.3. Lifshitz formula

The explicit form of the Green functions can be easily found for two parallel plates interacting via the long wavelength fluctuations. The simplest configuration is two semispaces made from different materials with the dielectric functions $\varepsilon_1(\omega)$ and $\varepsilon_2(\omega)$, respectively, separated by a small gap d filled with the material described by the dielectric function $\varepsilon_0(\omega)$. This configuration is shown schematically in Fig. 1.

2.3.1. Real frequency representation

For parallel plates the force (pressure) acting on body 2 (right plate) is calculated via the Green functions taken at $z = z' \to d/2$. Solution of Eq. (2.6) is very similar to the optical problem in the cavity with additional complication due to the tensor structure. The final result for the force (per unit area) can be written as

$$F(T,d) = \frac{\hbar}{2\pi^2}\int_0^\infty d\omega coth\left(\frac{\hbar\omega}{2kT}\right)\mathrm{Re}\int_0^\infty dq\; q\; k_0\; g(q,\omega), \tag{2.7}$$

where the wave vector in the gap is $\mathbf{K} = (\mathbf{q}, k_0)$ with $\mathbf{q}$ being the x and y components of the vector and $k_0 = (\varepsilon_0\omega^2/c^2 - q^2)^{1/2}$ being the z-component. The function $g(q,\omega)$ is

$$g(q,\omega) = \sum_{\nu=s,p}\frac{r_1^\nu r_2^\nu e^{2ik_0 d}}{1-r_1^\nu r_2^\nu e^{2ik_0 d}}. \tag{2.8}$$

Here $r^\nu_{1,2}$ are the reflection coefficients of the inner surfaces of the plates (index 1 or 2) for two different polarizations: $\nu = s$ or transverse electric (TE) polarization, and $\nu = p$ or transverse magnetic (TM) polarization. The factor $g(q,\omega)$ describes multiple reflections from the inner surfaces of bodies 1 and 2. The frequency dependent factor $coth(\hbar\omega/2kT)$ originates from the FDT.

The reflection coefficients $r^\nu_{1,2}$ entering in the Lifshitz formula are nothing else but the Fresnel reflection coefficients. In the simple configuration in Fig. 1 these coefficients are expressed via the z-component of the wave vectors in the gap k_0 and in the ith body k_i as

$$r_i^s = \frac{k_0-k_i}{k_0+k_i},\quad r_i^p = \frac{\varepsilon_i k_0-\varepsilon_0 k_i}{\varepsilon_i k_0+\varepsilon_0 k_i}, \tag{2.9}$$

where

$$k_0 = \sqrt{\varepsilon_0(\omega)\frac{\omega^2}{c^2}-q^2},\quad k_i = \sqrt{\varepsilon_i(\omega)\frac{\omega^2}{c^2}-q^2}. \tag{2.10}$$

Eq. (2.7) is the Lifshitz formula in the real frequency representation [33].

In many practical applications this representation is not very convenient because the integrand is a fast oscillating function due the factor $e^{ik_0 d}$. However, there are situations when the real frequency representation is the only possible or plays an important role in highlighting underlying physics. It happens, for example, in the non-equilibrium situations, when the plates have different temperatures [38]. In

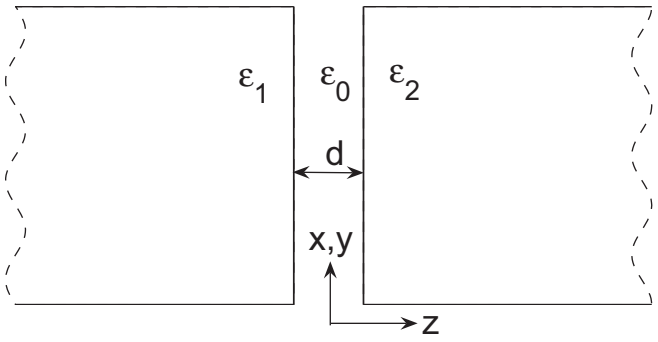

Fig. 1. The simplest configuration consisting of two semispaces separated by a gap, for which the Green function can be found explicitly.

addition, this paper is directed to the distance range $d \lesssim 100$ nm, where the thermal fluctuations do not play a significant role at T around the room temperature. This is because distance d is much smaller than the thermal wavelength $\lambda_T = \hbar c/kT = 7.6$ μm at $T = 300$ K. If we take into account only quantum fluctuations, then in Eq. (2.7) one has to change $coth(\hbar\omega/kT) \to 1$.

2.3.2. Imaginary frequency representation

The problem of fast oscillations is usually avoided by the contour rotation in the frequency complex plane. This is possible due to analyticity of the integrand. With this rotation the force can be expressed as an integral over the imaginary frequency $\omega = i\zeta$ as:

$$F(d) = \frac{\hbar}{2\pi^2}\int_0^\infty d\zeta \int_0^\infty dq\; q|k_0|g(q, i\zeta), \tag{2.11}$$

where the low temperature limit $T \to 0$ is assumed as explained above.

To get the reflection coefficients at imaginary frequencies one has to make analytical continuation of Eqs. (2.9) and (2.10) to the imaginary axis. For example, k_0 at $\omega = i\zeta$ will be

$$k_0 = i\sqrt{\varepsilon_0(i\zeta)\frac{\zeta^2}{c^2} + q^2}. \tag{2.12}$$

The general sign of the square root is defined by the condition that any wave decays inside of a material or $\mathrm{Im}k_0 > 0$. Therefore, the reflection coefficients in this case will depend on the dielectric functions at the imaginary frequencies $\varepsilon(i\zeta)$. These functions cannot be directly measured but can be expressed via the observable function $\varepsilon''(\omega)$ with the help of the Kramers–Kronig relation [33]:

$$\varepsilon(i\zeta) = 1 + \frac{2}{\pi}\int_0^\infty d\omega \frac{\omega\varepsilon''(\omega)}{\omega^2 + \zeta^2}. \tag{2.13}$$

The general property of $\varepsilon(i\zeta)$ is that this function is real, positive, and monotonously decreases when ζ increases.

The relation (2.13) shows that the dispersion forces are completely determined by $\varepsilon''(\omega)$, which is responsible for the dissipation in the material. Therefore, *the very existence of the forces is intimately related to the dissipation*. This relation is indeed a consequence of the fluctuation–dissipation theorem. The same Eq. (2.13) also shows that the force is sensitive to $\varepsilon''(\omega)$ in the integral sense.

2.3.3. Van der Waals and Casimir limits

Let us demonstrate that the Lifshitz formula (2.11) reproduces the van der Waals and Casimir regimes given by Eqs. (2.1) and (2.2) as limiting cases. Distance d separating the plates defines a characteristic imaginary frequency

$$\zeta_{ch} = c/2d. \tag{2.14}$$

It has to be stressed that *the real frequency $\omega_{ch} = c/2d$ does not always play a similar role due to fast oscillations of the integrand in Eq. (2.7).*

Let ω_{0i} be a typical frequency of the resonances in the absorption spectra of the i-th body or in the gap ($i = 0$). Distance d is so small that one can neglect the retardation $d \ll c/\omega_{0i}$ for every $i = 0, 1, 2$, then the van der Waals regime is realized because $|k_i| \approx |k_0|$. In this regime for the reflection coefficients one has

$$r_i^s \approx 0, \quad r_i^p \approx \frac{\varepsilon_i(i\zeta) - \varepsilon_0(i\zeta)}{\varepsilon_i(i\zeta) + \varepsilon_0(i\zeta)}. \tag{2.15}$$

It is interesting to note that the s-polarization does not contribute. It happens because in the quasi-static approximation, which is equivalent to the non-retarded case, the s-polarization is reduced to pure magnetic field that freely penetrates non-magnetic materials.

Introducing a new variable $x = 2d|k_0|$ it is easy to find from Eq. (2.11) with the help of Eq. (2.15)

$$F(d) = \frac{\hbar}{16\pi^2 d^3}\int_0^\infty d\zeta \int_0^\infty \frac{dx x^2}{\frac{(\varepsilon_1+\varepsilon_0)(\varepsilon_2+\varepsilon_0)}{(\varepsilon_1-\varepsilon_0)(\varepsilon_2-\varepsilon_0)}\, e^x - 1}, \quad d \ll \frac{c}{\omega_{0i}}, \tag{2.16}$$

where ε_i are functions of ζ. The double integral here depends only on the dielectric functions but not on the distance. Comparing Eq. (2.16) with the van der Waals force (Section 2.1.1) one finds that the Hamaker constant is defined as

$$A_H = \frac{3\hbar}{8\pi}\int_0^\infty d\zeta \int_0^\infty \frac{dx x^2}{\frac{(\varepsilon_1+\varepsilon_0)(\varepsilon_2+\varepsilon_0)}{(\varepsilon_1-\varepsilon_0)(\varepsilon_2-\varepsilon_0)}\, e^x - 1}. \tag{2.17}$$

This is a precise definition of the Hamaker constant expressed via the dielectric properties of involved materials.

In the opposite limit when the distance is so large that $d \gg c/\omega_{0i}$ (but still $d \ll \lambda_T$ to neglect the thermal effects) we can introduce new variables $x = 2d|k_0|$ and $p = x\zeta_{ch}/\zeta$ in Eq. (2.11). In these terms the argument of the dielectric functions $\varepsilon_i(i\zeta)$ will be $\zeta = \zeta_{ch}x/p$. By definition $p \geq 1$ and natural value of x is $x \sim 1$ due to the exponential dependence. It means that $\zeta \lesssim \zeta_{ch}$ and because ζ_{ch} is small we can take the static values of the dielectric functions $\varepsilon_i(i\zeta) \approx \varepsilon_{0i}$. With this simplification we can write Eq. (2.11) as

$$F(d) = \frac{\hbar c}{32\pi^2 d^4}\int_1^\infty \frac{dp}{p^2}\int_0^\infty dx x^3 g(x,p)\;|_{\varepsilon_i=\varepsilon_{0i}}, \quad \zeta_{ch} \ll \omega_{0i} \tag{2.18}$$

Again, the double integral here is a number that depends on permittivities of the materials. In this case both polarizations contribute and the force decreases faster with the distance increase due to the retardation effect. In comparison with the van der Waals force in Eq. (2.18) there is an extra factor ζ_{ch} responsible for the retardation. If we choose in Eq. (2.18) the materials to be ideal metals, $\varepsilon_{0i} \to \infty$ ($i = 1, 2$), and the gap to be vacuum, $\varepsilon_{00} = 1$, then both the reflection coefficients are $r_i^s = r_i^p = 1$ and we reproduce the Casimir result (Section 2.1.2).

Eqs. (2.16) and (2.18) present the limiting cases and these equations can be used only to obtain rough estimates in the range of separation typical for MEMS and NEMS. For example, for gold Eq. (2.16) can be applied with a reasonable precision for $d \lesssim 5$ nm [41] and Eq. (2.18) is working well for $d \sim 1$ μm [42] (for larger d the thermal correction becomes important). In the range of separation 1 nm $< d <$ 1 μm it is preferable to use full Eq. (2.11).

2.3.4. Convenient representation

Concluding the discussion of the Lifshitz formula let us present a representation convenient for numerical evaluation of the force. Introducing in Eq. (2.11) new variables x and t according to the relations $x = 2|k_0|d$ and $tx = \zeta/\zeta_{ch}$ the force can be presented in the form

$$F(d) = \frac{\hbar c}{32\pi^2 d^4}\sum_{\nu=s,p}\int_0^1 dt \int_0^\infty dx x^3 \frac{r_1^\nu r_2^\nu e^{-x}}{1 - r_1^\nu r_2^\nu e^{-x}}. \tag{2.19}$$

The Fresnel reflection coefficients are

$$r_i^s = \frac{1 - \sqrt{1 + t^2(\varepsilon_i - \varepsilon_0)}}{1 + \sqrt{1 + t^2(\varepsilon_i - \varepsilon_0)}}, \qquad r_i^p = \frac{\varepsilon_i - \varepsilon_0\sqrt{1 + t^2(\varepsilon_i - \varepsilon_0)}}{\varepsilon_i + \varepsilon_0\sqrt{1 + t^2(\varepsilon_i - \varepsilon_0)}}. \tag{2.20}$$

Here all the dielectric functions are functions of the imaginary frequency expressed via t and x as $\varepsilon_i(i\zeta) = \varepsilon_i(i\zeta_{ch}tx)$. The convenience of this representation is related to the simplicity of the integration range that is a stripe of unit width and effectively finite length.

The reflection coefficients (2.20) are presented for thick slabs made of material i. If the body i consists of different layers, then the reflection coefficients have to be generalized. For this case the coefficients can be found in Refs. [43,44].

2.4. Proximity force approximation

As was already mentioned, the force between two bodies can be presented in an explicit form only for parallel plates. While the stress tensor approach is valid for an arbitrary geometry of the bodies, the Green function cannot be found in a closed form. Recently numerical methods were developed [34] to evaluate the stress tensor for arbitrary geometries, but here a simple analytical approach is presented.

Under some conditions one can find approximate results for a non-planar geometry. This approximation, called the proximity force approximation (PFA), was applied for the first time for calculation of the dispersion forces by Derjaguin [45]. It was discussed in detail for applications in nuclear physics [46], and it was derived for bodies of arbitrary shapes in colloidal science [47]. The approximation can be applied when the smallest separation between bodies d is much smaller than a typical curvature R of the bodies [48], $d \ll R$. If this condition is fulfilled, locally one can change the curved surfaces by flat patches, calculate the force between the opposed patches as between parallel plates, and take the sum over all patches. The scheme of the procedure is presented in Fig. 2.

The size of patches must be much larger than d. If this size is still small in comparison with R, then one can change the sum over the patches by the integral. The precision of the PFA is of the order of d/R and the main problem of this approximation is that the precision is poorly controlled. The PFA can be also applied to other nonadditive forces. For example, one can apply it to the electrostatic force, for which the answers for some problems are known precisely [49].

Let us consider as an illustrative example the electrostatic force between a cylinder parallel to a plate. The force (per unit area) between two plates in a vacuum is

$$F_{el}^{pl}(d) = \frac{V_0^2}{8\pi d^2}, \tag{2.21}$$

where V_0 is the potential difference between the plates. The local distance between the cylinder and the plate is $d(x) = R + d - (R^2 - x^2)^{1/2}$, where R is the radius of the cylinder and x is the horizontal coordinate in the plane of Fig. 2. The local distance can be approximated as $d(x) \approx d + x^2/2R$. The area of rectangular patches is $dA = Ldx$, where L is the length of the cylinder. Then the force between the cylinder and the plate within PFA will be

$$F_{el}^{c,pl}(d) \approx \frac{V_0^2}{8\pi}\int_{-\infty}^{\infty}\frac{Ldx}{\left(d + x^2/2R\right)^2} = \frac{V_0^2 L\sqrt{R}}{8\sqrt{2}d^{3/2}}, \tag{2.22}$$

where we changed the integration limits to infinity within the precision d/R. The precise electrostatic result is [50]:

$$F_{el}^{c,pl}(d) = \frac{LV_0^2}{\Delta} ln^{-2}\left(\frac{d+R-\Delta}{d+R+\Delta}\right), \tag{2.23}$$

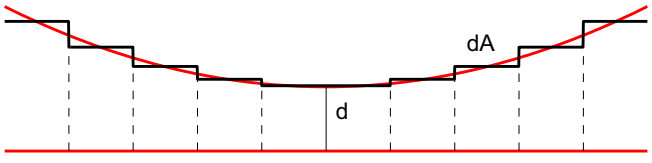

Fig. 2. Scheme of application of the proximity force approximation.

where $\Delta = [(d+R)^2 - R^2]^{1/2}$. Expanding Eq. (2.23) in a series of d/R one finds that the relative correction to PFA result (2.22) is $9/8(d/R)$. The latter is in agreement with the expectations.

The PFA was invented to calculate the dispersion forces in the configurations of sphere–plate and crossed cylinders that were used to measure the forces. In both cases the van der Waals and Casimir forces calculated from the plate–plate interaction (Section 2.1.1) and (Section 2.1.2) are

$$F_{vdW} = \frac{A_H R}{6d^2}, \quad F_C(d) = \frac{\pi^3 R}{360}\cdot\frac{\hbar c}{d^3}. \tag{2.24}$$

For the sphere–plate configuration R is the radius of the sphere and for the crossed cylinders $R = \sqrt{R_1 R_2}$, where R_1 and R_2 are the radii of cylinders.

The PFA integration can be applied to the Lifshitz formula (2.11) to find the force between sphere and plate. In this formula the dependence on the distance d is contained in the exponent $e^{-d|k_0|}$. This distance has to be changed by the local distance $d(x, y)$ and the formula has to be integrated over the (infinite) area in x–y plane. After explicit integration one finds:

$$F^{sp}(d) = -\frac{\hbar R}{2\pi}\sum_{\nu=s,p}\int_0^\infty d\zeta\int_0^\infty dqql n\left(\frac{r_1^\nu r_2^\nu e^{-2|k_0|d}}{1-r_1^\nu r_2^\nu e^{-2|k_0|d}}\right). \tag{2.25}$$

This equation is usually considered as the Lifshitz formula for the sphere–plate configuration at zero temperature.

3. Critical experiments

The importance of roughness on dispersion forces has been fully recognized relatively recently. This recognition was ignited by a few critical experiments performed in different fields where these forces play important role. In this chapter we describe these experiments and review related papers.

3.1. Forces between corrugated bodies

In this section we consider the dispersion interaction with intentionally corrugated bodies. It differs from random surface roughness but firmly establishes nonadditivity of dispersion forces that is used further for random roughness.

The Casimir force is strongly geometry dependent [22,51,52] and it was already stressed that the dispersion forces in general are not additive. One of the well-investigated case is the interaction between a flat plate and a corrugated plate. The force between flat and sinusoidally corrugated plates made of ideal metal was calculated for the first time in Ref. [52] taking into account non-additivity effects (beyond the proximity force approximation). It was found that for corrugation wavelength λ much larger than the distance between bodies $\lambda \gg d$, the pairwise summation works well but in the opposite limit, $\lambda \ll d$, the deviation from PFA is significant. The case of rectangular corrugation was considered in [53]. Strong deviation from PFA was found over a wide range of λ, even though the surface was composed only of flat segments.

Strong deviation from PFA for rectangular corrugation one can understand qualitatively in the following way. The Casimir force is associated with confined electromagnetic modes with wavelength comparable to the separation between the interacting objects. When $\lambda \ll d$ these modes fail to penetrate into the trenches, rendering the Casimir force on the corrugated surface equal to a flat one. On the other hand, for sufficiently deep trenches the additivity predicts the effective area of interaction that is equal to the fraction of solid surface.

Besides many theoretical arguments the nonadditivity was tested only recently by direct experiments. For these experiments corrugated plates provide a convenient platform. The first experiment where the

normal Casimir force between aluminum-coated plate with small sinusoidal corrugation and a large sphere was performed with the use of an atomic force microscope technique [54]. The force was measured in the range of separations between the bodies from 0.1 to 0.9 μm. While this measurement showed deviations from PFA, the interpretation of the deviation is still controversial [52,55].

The first conclusive experiment has been done by Chan et al. in 2008 [56] (see also [57]). In this experiment one of the interacting objects is a silicon plate with nanoscale high aspect ratio rectangular corrugations. The other object was a gold-coated glass ball with a radius of 50 μm. Two identical balls are stacked and glued onto a micromechanical torsional oscillator [58,59] that is often used to measure the Casimir force. The oscillator consisted of a 3.5 μm thick, 500 μm square silicon plate suspended by two torsional rods. Some details of the experimental configuration are shown in Fig. 3.

Three plates were used for measurements: one with a corrugation period of 400 nm, one with a period of 1 μm, and one with a flat surface. The distance between the ball and the plate was varied with a piezoelectric actuator. The resonance frequency of the torsional oscillator was changed in response to the attraction between the ball and the plate. This frequency change is proportional to the gradient of the force between bodies.

It was found that for the flat sample the measured force is in a reasonable agreement with the force predicted theoretically. The latter was calculated using the Lifshitz formula for sphere–plate (2.25) with the tabulated optical data [60] for used materials (Au and Si). Note that roughness of gold layer on the sphere can be neglected because it was small in comparison with the distance between bodies. For the sample with a corrugation period of $\lambda = 400$ the measured gradient of the force $F'(d)$ is shown in Fig. 4a. The observed value is compared with the force gradient predicted by PFA that is $pF_{flat}'(d)$, where $p = 0.5$ is the fraction of solid surface on the sample and $F_{flat}(d)$ is the force for the flat sample. One can see that the measured force gradient is larger than that predicted assuming the additivity. Fig. 4b shows the parameter

$$\rho(d) = \frac{F'(d)}{pF'_{flat}(d)}. \tag{3.1}$$

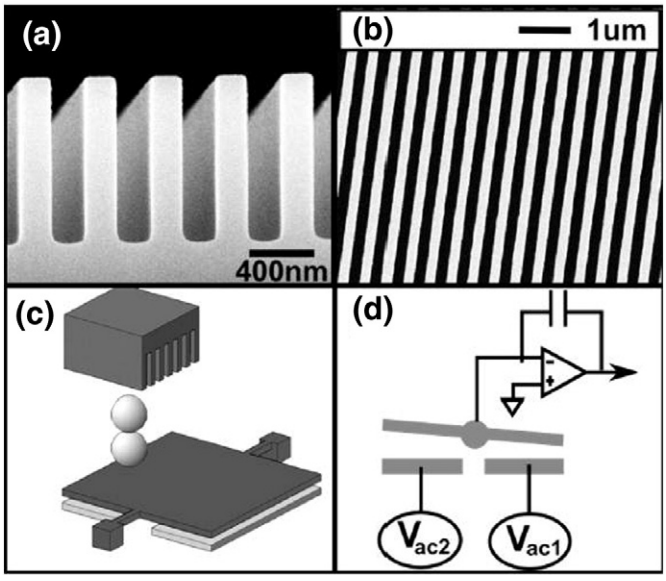

Fig. 3. Detail of the experiment [56]. (a) Cross section of rectangular trenches in silicon with a period of 400 nm and depth of 0.98 μm. (b) Top view of the trenches. (c) Scheme of the experimental setup including the torsional oscillator, gold covered spheres, and silicon trench array. (d) Measurement scheme with electrical connections.
Courtesy of H. B. Chan.

Deviation of this parameter from 1 characterizes the effect of nonadditivity. One can see that this deviation is more than 20%, however, it is less than the value predicted theoretically [53] for perfect reflectors. It was concluded [56] that both effects nonadditivity and finite conductivity of the materials play a role.

In the PFA picture, the total interaction is a sum of two contributions: interaction with the top surface of the corrugated plate (fraction p) and interaction with the bottom surface (fraction $1 - p$). In the experiment [56] the latter contribution is negligible because the trenches are deep (~ 1 μm) and interaction with the bottom surface is small. In Ref. [61] the depth of trenches was comparable with the distance between bodies and the contribution of the bottom surface played a role. The measured force was compared with advanced calculations based on the scattering theory [34,62,63] that includes both geometry effects and the optical properties of the material. In this experiment a reasonable agreement with the theory was found. Therefore, nonadditivity of dispersion forces is now proven experimentally and is in a good agreement with theoretical expectations.

Recently a detailed investigation of interaction between metallic gratings with the sizes on the level of 100 nm and a sphere was performed [64]. Corrugations in a metallic layer can behave differently from that in Si because collective surface modes such as surface plasmons can be excited in metallic gratings. It is known that the surface plasmons affect the force in a non-trivia manner [65]. Very significant deviations from the PFA predictions were observed, however, the interpretation of these deviations is still unclear.

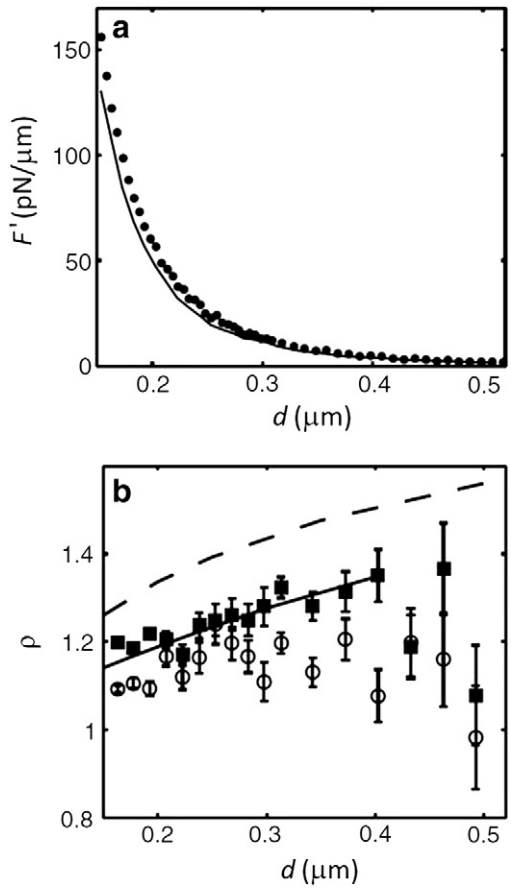

Fig. 4. Results of the experiment [56]. (a) Measured gradient of the Casimir force (dots). The solid curve is the theoretical prediction assuming additivity but taking into account finite conductivity of the material. (b) Parameter ρ defined by Eq. (3.1). Experimental data for $\lambda = 400$ are shown by solid squares and for $\lambda = 1$ μm are shown by open circles. The theoretical predictions are shown by the dashed and solid lines for the first and second case, respectively.
Courtesy of H. B. Chan.

3.2. Stiction problem

Because of the very small sizes involved in micro and nanoelectromechanical systems (MEMS or NEMS), surface forces are dominant, and they can generate a severe problem resulting in malfunction some of the MEMS devices or making fabrication impossible. The problem is spontaneous stiction between separate elements of MEMS devices. It is an important limitation in bringing MEMS to the broader market. The problem was identified already in the 1990s [16,66,67]. MEMS structures are typically made by forming a layer of material on top of a sacrificial layer above another material with the following wet etching of the sacrificial layer. For example, it is desirable to fabricate transducers with suspended structures that have a minimum gap distance and large area. Drying after rinsing is the final fabrication step that can collapse such microstructures resulting in permanent adherence. Schematically the situation is shown in Fig. 5. Strong capillary forces pull the surfaces together but when the liquid is dried out the surfaces can stuck permanently due to presence of the dispersion forces. It happens if a restoring elastic force cannot overcome attraction induced by the dispersion forces.

This strongly undesirable effect makes impossible fabrication of many MEMS devices or restricts their functioning. The latter happens if two surfaces approach too close to each other during the device operation. The reason can be related to surface forces (capillary, electrostatic) or inertial forces (shock, rapid air flow). Due to jump to contact the surfaces stuck permanently and the device cannot operate anymore. Fig. 6 shows failures of realistic MEMS devices. It was realized that coating materials, surface roughness, and environmental aging can influence the autoadhesion.

The problem of adhesion between macromachined surfaces was tackled experimentally using microfabricated cantilevers hanging above a substrate [17,69–71]. A theory and experimental method for measuring surface energy of cantilever beams has been proposed by Mastrangelo and Hsu [72,73]. This theory describes the role of capillary forces in bringing beams into contact with the substrate and determines critical beam lengths for beam collapse. Adhesion of the dried cantilever beam is predicted by considering the elastic energy in the deformed beam, which is attempting to pull the beam up off the substrate, and the surface energy that is promoting continued adhesion.

The theory was refined further by de Boer and Michalske [69] who proposed and realized also a practical method to measure the adhesion energy. They fabricated an array of cantilever beams made of polysilicon. The beams with a width of 20 μm were separated from Si substrate by a gap of 1.8 μm and their length was varied from 10 to 500 μm. One set of samples was dried in air after rinsing and the other set was treated with a molecular coating of octadecyltrichlorosilane. The samples from the first set were hydrophilic and from the second set were hydrophobic.

Short beams were free but starting from some length (172 and 225 μm for hydrophilic and hydrophobic, respectively) the beams were adhered. The adhered cantilevers had so-called S-shape shown in Fig. 7a. According to the theory [69,72] from the shape of the beams one can deduce the adhesion energy. An important parameter here is the crack length s that is an unattached length of the beam. The attached length t can be calculated as $t = L - s$, where L is the length of the beam. The shape of adhered cantilevers was observed with the help of an interferometer. Interferograms similar to those in Fig. 7b–e were recorded and analyzed. It was shown that the shape of S-shaped cantilevers is in

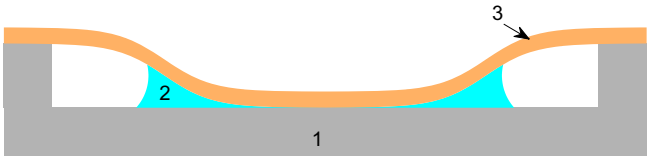

Fig. 5. Schematic view of a membrane suspended above a substrate. 1 is the substrate, 2 is liquid, and 3 is the membrane. Drying meniscus pulls the surfaces together. When the liquid is vaporized the membrane can stuck to the substrate if the restoring elastic force is smaller than the dispersion forces acting on the membrane.

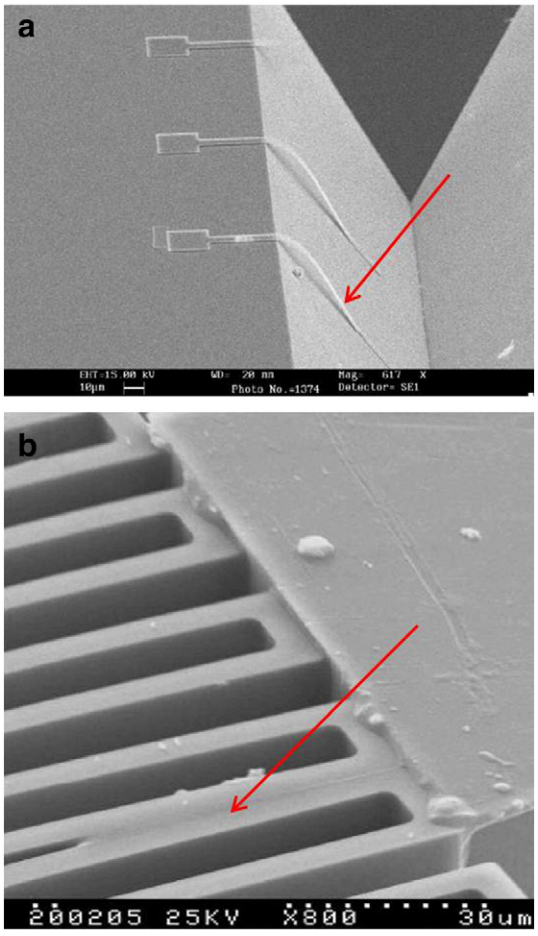

Fig. 6. Permanent stiction in MEMS devices [68]. The arrows show adhered elements. (a) Stiction of soft microcantilevers to the substrate. (b) Microstructured elements in a micromachined accelerometer after impact loading.
Courtesy of Y. P. Zhao.

good agreement with expectations and can be used for precise determination of the adhesion energy. Although the surface roughness in this experiment was not changed, it was stressed that it can play a significant role in the apparent adhesion energy.

Controlled actuation of cantilevers was used [70,71] instead of spontaneous adhesion to get more detailed information on the surface forces acting in the adhesion area (landing pad). For this purpose an actuation pad under each beam was fabricated [74]. The cantilever and landing pad were at ground potential, while a large potential can be applied to the actuation pad (see Fig. 7a). Detailed theoretical description and measurement of the beam shape under combined action of the electrostatic and adhesive forces was made in Ref. [71].

Chemical and capillary forces result in the strongest adhesion between surfaces [75] but these forces can be eliminated using coating with a low-surface-energy hydrophobic molecular monolayer [76,77]. However, the dispersion forces cannot be eliminated and they pose a fundamental limit to the adhesion between micromachined surfaces. Influence of surface roughness on the adhesion energy was investigated in a special experiment with the actuated cantilevers [17]. The main purpose of this experiment was to clarify the role of the van der Walls forces in adhesion of micromachined surfaces.

Polysilicon cantilevers 1500 μm long and 30 μm wide separated from the substrate by a gap of 1.9 μm were used in this experiment. To make the cantilevers freestanding and also to eliminate capillary forces at the interface, a hydrophobic monolayer coating of perfluorodecyltrichlorosilane (FDTS, $CF_3(CF_2)_7(CH_2)_2SiCl_3$) was applied with a water contact angle of 110° in a solvent-based process [76]. Roughness of the lower layer

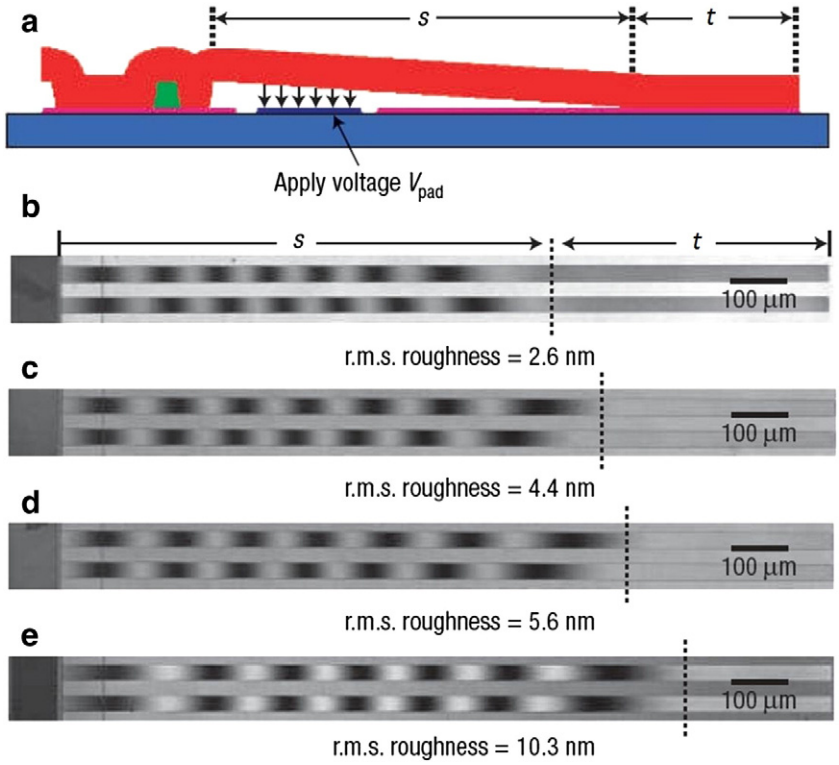

Fig. 7. Adhered cantilever [17]. (a) Schematic image of the cantilever adhered to the substrate. The crack length is *s*, the adhered length is *t*. Voltage can be applied to the actuation pad to produce an electrostatic load. (b)–(e) Interferograms of cantilever beams at a fixed actuation voltage but different surface roughnesses.
Courtesy of M. P. de Boer.

of polysilicon, which defines the landing pad, was accomplished by thermal oxidation in dry O_2 at 900 °C for increasing times. The rms surface roughness increases with the oxidation time. This occurs because the polysilicon grains are randomly oriented, and dry oxidation proceeds at different rates on the various orientations of silicon.

To perform the adhesion test freestanding cantilevers were brought into contact with the substrate by applying a voltage to the actuation pad. Using phase-stepping interferometry, the full deflection curve of the cantilevers was determined to nanometer-scale accuracy. The resulting interferograms are shown in Fig. 7b–e for an applied load of $V_{pad} = 50$ V. They qualitatively indicate a decrease in adhesion for an increase in surface roughness. The adhesion energy was extracted from the beam shape under action of electrostatic and adhesive forces as described in [71].

The result is presented in Fig. 8 as a function of the average surface separation d_{ave} that was calculated using actual surface topography (see [17] for details). For relatively smooth surfaces it is natural to assume that the adhesion energy per unit area Γ is defined by the dispersion forces between parallel plates separated by the distance d_{ave} [74]. This distance (later we call it distance upon contact) is defined by one highest asperity where the bodies come to a contact. The energy due to the van der Waals force in the contact area is negligible in comparison with that in the non-contact area. This limit case is shown by the blue curve. The other limit case is realized for relatively rough surfaces when the dispersion force over the non-contact area is negligible. In this case the adhesion energy is given by the van der Walls interaction in the area of contact. It is estimated as [13]

$$\Gamma = \frac{1}{A}\left(\frac{A_H R}{6d_0}\right), \tag{3.2}$$

where A is the nominal area of contact, R is the radius of contacting asperity, and $d_0 = 0.2$ is the cutoff separation. This limit is shown in Fig. 8 by a black line.

Influence of surface roughness on Γ was estimated using the actual surface topographies of the landing-pad and structural polysilicon layers. The topographies were measured by tapping-mode atomic force microscopy (AFM). For each pixel in the AFM images the local distance d_{loc} was determined. The surface energy was calculated as the sum of dispersion energies over all pixels opposing each other. These calculations are shown by the green triangles in Fig. 8. At last the experimental results for Γ determined from the shape of cantilevers are presented by brown squares.

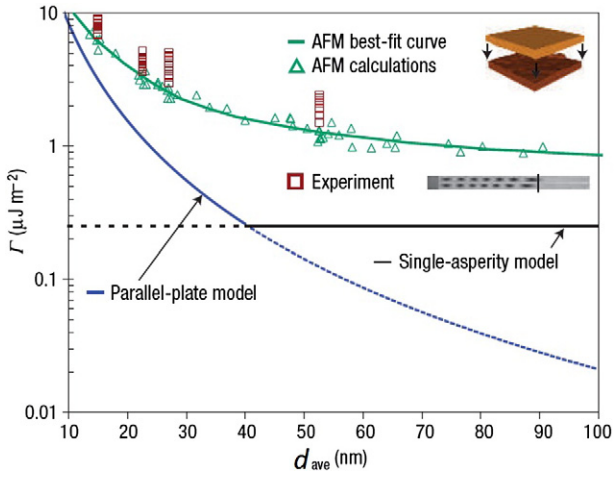

Fig. 8. Adhesion energy as a function of averaged distance between rough bodies [17]. The blue curve shows the limit of smooth surfaces separated by the distance d_{ave}. The black line gives the adhesion energy for the limit of single asperity contact. The triangles show the energy calculated from the AFM images and the squares give the energy determined from the observed shapes of cantilevers.
Courtesy of M. P. de Boer.

In Fig. 8 one can conclude that the energy determined experimentally and that estimated from the AFM images are in a reasonable agreement with each other. However the limits of smooth surfaces and single asperity contact lie well below the experimental data. It means that the surface roughness gives a considerable contribution to the adhesion energy and simple theoretical models strongly underestimate Γ. The situation does not change for a relative humidity up to 80%, therefore, capillary condensation does not play a role.

3.3. Forces measured with surface force apparatus

Dispersion interaction across liquid medium is often accompanied by the electrostatic interaction. Both of these interactions are nonadditive and for this reason the inclusion of roughness into consideration is a difficult problem. Despite the fact that most of natural surfaces are rough, in very few experiments the influence of surface roughness on the dispersion forces was reported.

Two main methods to measure the dispersion forces in liquid environment are in use. One uses a surface force apparatus (SFA) where the force is measured between two macroscopically curved surfaces over a relatively large area of nominal contact. This method is able to measure absolute normal distances with angstrom resolution. The second method uses AFM to measure the forces. In this case the interaction area is much smaller and determination of the absolute separation between bodies is a difficult problem. We consider the second method in the next section.

With the help of SFA the effect of surface roughness on the contact mechanics was studied for various polymeric surfaces with application of external load [78]. The force was measured in the crossed-cylinder geometry with a curvature radius of $R \approx 2$ cm. Experiments were conducted in atmosphere of dry nitrogen or with lubricant oil between surfaces. Randomly rough surfaces were prepared by spin coating of polymer films onto mica. Roughness was controlled by varying the temperature of the polymer solution, the solvent composition, the rate of evaporation, and the relative humidity when deposited onto a substrate. The rms roughness was varied from 3 to 220 nm.

Normal force-distance curves measured on several different randomly rough surfaces all show an extended exponentially repulsive force at close distances. The repulsion is dominated by asperities and their bulk elastic or plastic properties. At large separations, the forces were less repulsive due to the attractive short-range van der Waals and/or solvation forces between the initially contacting asperities. The adhesion energy versus roughness showed no obvious correlation at a fixed preload. Moreover, the observed value of adhesion was very large, $\Gamma \approx 28$ mJ/m^2. For comparison, the value of Γ between oxidized polysilicon surfaces [17] was smaller than 10 μJ/m^2. Large adhesion energy was explained by the segmental entanglements of the polymers, which is correlated with the real contact area [79]. The results of the discussed paper are consistent with the old statement [80] that the real contact area is proportional to the applied load and with the later works [81,82] on the effect of roughness and material stiffness on the adhesion of solids.

A different method to prepare rough surfaces was used in Ref. [83]. The rough surfaces were polymer replicas of substrates of different roughness and composition. The replicas were fabricated following a technique similar to microcontact printing [84], using a UV-curable polyurethane. This method made it possible to keep the mechanical properties and surface chemistry of the substrates constant, while varying the roughness. The friction between surfaces prepared in this way and smooth bare mica was measured in dry air or in the presence of lubricating oil using the SFA.

The experiments described in [78,83] are related to the main point of our interest but do not tell much on the roughness dependence of the dispersion forces. This is because the adhesion investigated in these papers was not dominated by the dispersion forces as, for example, in [17] but was defined by much stronger forces related to the segmental entanglements of the polymers.

There is lack of unambiguous experimental data on interaction forces between rough surfaces in electrolyte solutions. The first surface force measurements across a liquid medium between a rough metal and a ceramic surface with a control of the electrochemical potential was performed in Ref. [85]. These experiments reveal how increasing level of surface roughness and dissimilarity between the potentials of the interacting surfaces influence the strength and range of electric double layer, dispersion forces, hydration, and steric forces and how this contributes to deviations from DLVO theory (other than roughness deviations are reviewed in [15]). Roughness and hydration effects [86] are known to influence colloidal forces, adhesion, contact mechanics, friction and wear [87,88].

An electrochemical surface force apparatus (EC-SFA) was used to control interaction forces between dissimilar surfaces in situ in an electrolyte [89]. This apparatus is well suited to study the forces between rough electrodes. It has combined capabilities to simultaneously control the electrode surface potential, measure interaction forces, and visualize the contact mechanics. The system used for measurements in Ref. [85] is illustrated in Fig. 9. The forces were measured between gold electrode with varied surface roughness and a molecularly smooth self-assembled amino-silane monolayer on mica in a 1.0 mM aqueous solution of HNO_3. The surface potential of the gold electrode was varied in situ. Three samples with different roughness were used. One sample was atomically smooth gold film (Au-1) with rms roughness $w = 3$ Å prepared by template stripping from mica surface [90]. The second sample (Au-2) was prepared by physical vapor deposition (PVD) and was moderately rough ($w = 12$ Å). The third sample (Au-3) was further roughened by electrochemical treatment of the deposited Au film ($w = 17$ Å). Although the third sample is only slightly rougher compared to the second one, it has a distinctly different surface morphology.

Fig. 10 shows the force-distance profiles measured for positive electrode potentials ($\Delta U > 0$), where the electrode and SAM surfaces are like-charged (the amine groups in SAM are fully protonated charging the surface positively). The results show that interaction forces measured for atomically smooth gold surfaces are fitted very well by DLVO-theory using constant potential boundary conditions down to separations of

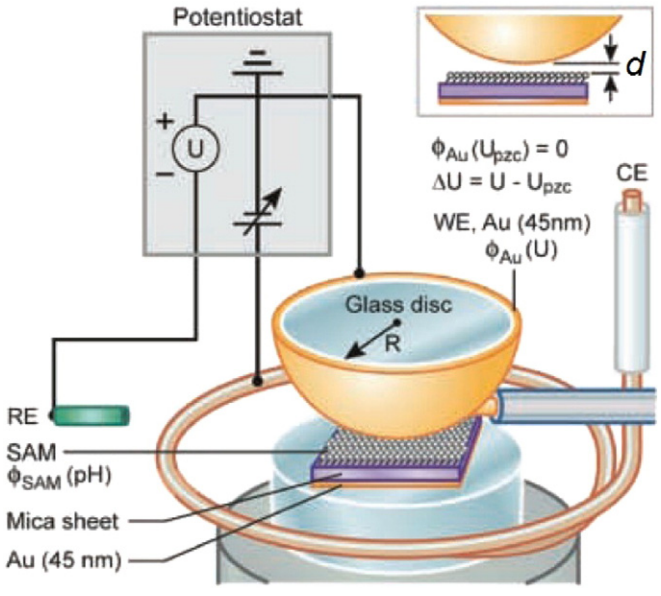

Fig. 9. Scheme of the experiment with the electrochemical SFA [85]. The electrochemical three-electrode cell consists of the gold working electrodes (WE), a platinum counter electrode (CE), and an Ag|AgCl reference electrode. The WE is a glass sphere or cylinder covered with gold. Interaction of the WE is investigated with the mica sheet covered with amino-silane monolayer. In this setup an external electrochemical potential is applied to the gold electrode and force–distance curves are measured. At the potential U_{pzc} (the potential of zero charge) the effective surface potential of gold is zero.
Courtesy of J. N. Israelachvili.

around 8 nm. Below 8 nm, the Au-1 electrode shows a jump in to about 4 nm, where the appearance of short ranged hydration forces overpowers the attractive contribution from the dispersion forces. The solid line describing the fit for Au-1 data includes DLVO interactions and an additional term taking into account repulsions due to hydration forces. This repulsive contribution agrees well with the literature value [91] for specifically adsorbed nitrate ions at the positively charged SAM surface.

The force profiles and the repulsive 'hard wall' separation measured for the two rough surfaces are shifted outwards by approximately 3 nm and 3.5 nm for Au-2 and Au-3, respectively. Moreover, an additional exponentially repulsive component is superimposed on the force profile (see Fig. 10) for rough samples and a pronounced 'kink' in the slope of the repulsive force can be seen. These effects represent an additional steric repulsion force arising from the elastic deformation of the outermost asperities at the rough surfaces. These asperities extend out to up to 10–15 nm.

It was found also that even small differences in the roughness morphology lead to observable changes in the force profiles. Particularly, the differences in "jump-in" behavior show that attractive dispersion forces are weakened by the presence of surface roughness and depend on the height distribution and number density of the nano-scale asperities. Qualitatively similar effects were observed for opposite charged surfaces ($\Delta U < 0$).

It has to be noted that in general the surface force apparatus are better suited for investigation of surface forces at very small separations and assume application of significant load. In comparison with the force measurements with AFM they investigate larger area and independently measure the distance between bodies with high precision. On the other hand, the AFM method can give more detailed information about the force at larger separation without application of external load. This method is reviewed in the next section.

3.4. Forces measured with atomic force microscope

Precise measurement of the dispersion forces with AFM was performed for the first time by Mohideen and Roy in 1998 [92]. A typical scheme for AFM experiments is shown in Fig. 11. Instead of a sharp tip they attached a sphere to the AFM cantilever to increase the magnitude of the force. For this configuration the effective area of interaction is $\sim \pi R d$, where R is the sphere radius. For practical reasons it was possible to use the sphere with a radius of 100 μm. The interaction area is much smaller than that in SFA where $R = 2$ but with a soft cantilever (spring constant $k \approx 0.02$) it was possible to measure quite weak forces ~ 10. In this experiment both the sphere and the plate were covered with 300 nm of aluminum and 20 nm of Au/Pd alloy to prevent oxidation of Al. The distance between bodies was controlled with a piezo.

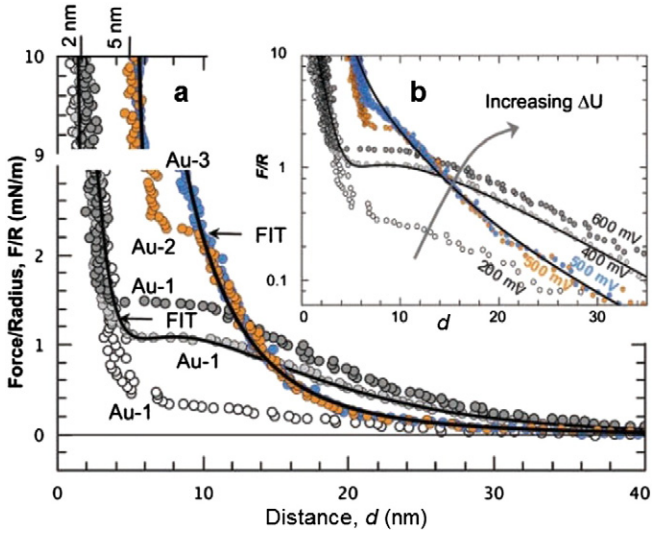

Fig. 10. Results of the experiment [85]. (a) Representative force–distance profiles measured during approach at externally applied positive potentials ($\Delta U = U - U_{pzc}$). Differently rough gold electrodes are indicated as Au-1,2,3. The inset (b) shows the semi-log plot of the same data shown in (a). The solid lines correspond to theoretical fits (normalized by the radius of curvature, R) using the theoretical model explained in [85]. Courtesy of J. N. Israelachvili.

The main problem of the AFM method is determination of the absolute distance between the bodies. It is reduced to determination of the parameter d_0 that is the absolute separation on contact. This parameter is usually extracted from the electrostatic force measured at relatively large distances where the dispersion forces are small. Significant progress in determination of d_0 was reached during later development [58,93,94] but the errors in the force versus separation distance are still dominated by the errors in d_0.

In the first experiment [92] roughness of the bodies was quite significant up to 35 nm on each surface. As the result the distance upon contact was determined as $d_0 = 120 \pm 5$. In this situation roughness has to give a significant contribution to the force. It was estimated using the perturbation theory (see Section 4.2) as 50% at closest separations. In the following development of the method most of the experiments were performed using Au [95] instead of Al to cover the dielectric bodies. This eliminated the problem of oxide formation and resulted in significant reduction of roughness applying well-developed deposition methods. In the most precise experiments [59,95–96] the roughness contribution to the force was on the level of the experimental errors.

However, the precise experiments were performed at distances of the order of 100 nm. In this case rms roughness in a few nanometers is not important but at smaller separations it can play very significant role. Special investigation of the roughness effect at smallest possible separations was undertaken in Ref. [26] (see some additional details in [97]). Relatively stiff cantilevers have been used to reach as small separations as possible between sphere ($R = 100$ μm) and plate before jump to contact. The sphere was covered with 100 nm Au in an electron-beam evaporator. Silicon wafers were coated in the same way by Au to different thicknesses between 100 and 1600 nm. All of these films have different rms roughness w and different feature size ξ (correlation length) as one can see Fig. 12. The value of w increases with the film thickness from 1.5 nm to 10.1 nm while ξ is between 22 and 42.

The force was measured in air in the same way as shown in Fig. 11. The cantilever spring constant k, the residual contact potential V_c, and the distance upon contact d_0 all three parameters were determined from the electrostatic calibration similar to [95]. Much stiffer cantilevers with $k =$ 0.235 have been used. It was found that the parameter d_0 correlates very well with the roughness of investigated surfaces. Nearly linear

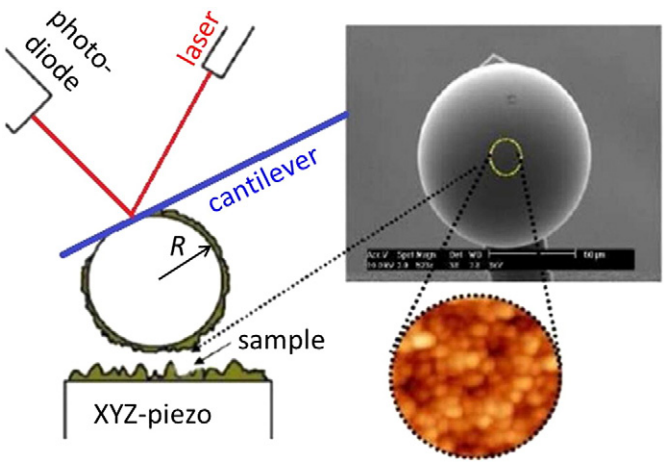

Fig. 11. Scheme of the AFM experiment. The sphere is attached to the AFM cantilever whose position is read out by a laser beam. The plate is mounted on a piezo allowing control of the distance between bodies. Inset shows SEM image of the sphere with magnified area shown as AFM image.

relation (see inset in Fig. 13) was found $d_0 = C(w + w_{sph})$, where $w_{sph} = 3.5$ is the sphere roughness and the constant $C \approx 3.7$. It is important to stress that the value of d_0 is considerably larger than the rms roughness of interacting surfaces. At the smallest possible separations (just before jump to contact) the error in the force versus separation d is about 10% and it is dominated by the error in d_0 that is $\Delta d_0 \sim 1$.

The results for the force vs distance are presented in Fig. 13 for the films of different thicknesses. Thin films (100, 200, and 400 nm) are in reasonable agreement with the theoretical expectations that take into account some deviations of dielectric functions of deposited gold from the single crystal material and account for the roughness corrections using the perturbation theory (see Section 4.2). For these films the force is well described by the power law [98] $F \sim d^{-\alpha}$, where α is between 2 and 3. However, the thick films show very different behavior. There is significant deviation from expected scaling. The theoretical curve (black) including the roughness correction is not able to describe the observed force. It seems like the perturbation theory is still applicable even for the roughest film 1600 nm. For this film $w \approx 10$ and the minimal distance is $d = d_0 \approx 50$. The relative perturbation correction is estimated as $6(w/d_0)^2 \approx 0.24$. It is much smaller than the observed deviation. Explanation of this phenomenon is presented in Section 4.3.

The force in the sphere–plate configuration was measured with AFM also in intervening liquids. Munday and Capasso [99] measured the force between gold covered bodies in ethanol. In polar liquids electrostatic calibration of the system (determination of k, V_c and d_0) is inappropriate due to strong reduction of the force. Instead the hydrodynamic drag force has been used for calibration. In this experiment the force was measured for distances as small as 35 nm and the effect of surface roughness clearly manifested itself in the data. It was found that a simple theory for roughness correction based on PRA (see Section 4.2) overestimates the force at small separations. Few information on the roughness morphology was presented. A more detailed analysis of the electrostatic forces has been done in [100] including the screening effect due to dissolved NaI in ethanol. In this experiment the measured force was found to be in a good agreement with the theoretical prediction including the roughness correction. Comparison of the dispersion forces between gold–gold and gold–silica immersed in bromobenzene is discussed in [101]. It was observed that the force between gold and silica becomes repulsive as predicted by the Lifshitz theory. The roughness contributed to the force was not discussed in detail.

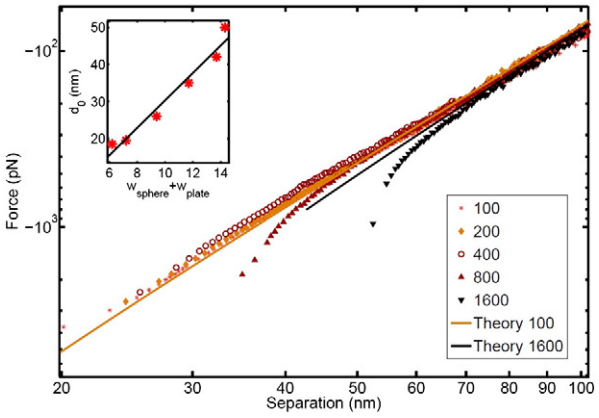

Fig. 13. Casimir force measured for different rough surfaces on a log–log scale for various Au film thicknesses. The theoretical curves for 100 nm and 1600 nm films are shown by solid lines. The inset shows the electrostatically calibrated values of d_0 as a function of the rms roughness.

3.5. What we learned from the experiments

The first conclusion that can be driven from the experiments with corrugated bodies is that the dispersion forces are not additive. In general, one cannot calculate the force using the pairwise summation method. Instead much more complicated approaches developed in the last 15 years have to be used. The additivity is applicable if the corrugation wavelength is much larger than the distance between bodies. It is not very clear to what extend we can transfer this conclusions to random roughness.

Both AFM experiments in air and experiments with adhered cantilevers demonstrate that the dispersion forces deviate very significantly from expectations based on simple theories. Typically the forces at small separations are much larger than expected. The situation for interaction in liquids is not that clear and needs more analysis.

Experiments with SFA give very detailed information about the forces for bodies in contact at significant external load. When the separation distance increases they become less informative. An important conclusion that can be drawn from these experiments is significant influence of roughness distribution on the dispersion forces.

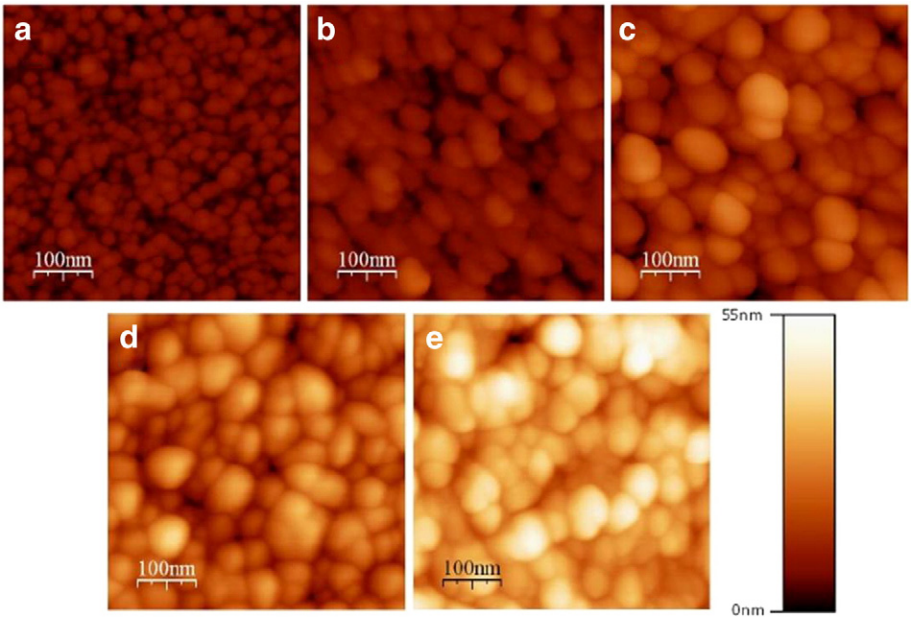

Fig. 12. AFM images of deposited Au films on Si substrate. Successive images correspond to the film thickness 100, 200, 400, 800, 1600 nm, scan size is 0.5 μm, all but the last on the same color scale.

4. Theoretical description of roughness

The Lifshitz formula (2.19) does not take into account inevitable roughness of interacting bodies. When rms roughness of the bodies is much smaller than the separation distance, then the roughness influence on the force can be calculated using the perturbation theory (see Section 4.2). However, when the distance becomes comparable with the roughness, the perturbation theory cannot be applied. The problem of short distance separations between rough bodies is one of the unresolved problems. In this chapter we give introduction into interaction of two rough plates or a sphere and a plate and describe the current state of the problem.

4.1. Description of a rough surface

4.1.1. Characterization

Suppose there is a rough plate with a surface profile that can be described by the function $h(x, y)$, where x and y are the in-plane coordinates. An approximation for this function provides, for example, an AFM scan of the surface. It gives the height h_{ij} at the pixel position $x_i = \Delta \cdot i$ and $y_j = \Delta \cdot j$, where $i, j = 1, 2, \ldots, N$ and Δ is the pixel size related to the scan size as $L = \Delta \cdot N$. We can define the mean plane of the rough plate as the averaged value of the function $h(x, y)$: $\overline{h} = A^{-1} \int dxdyh(x, y)$, where A is the area of the plate. This definition assumes that the plate is infinite. In reality we have to deal with a scan of finite size, for which the mean plane is at

$$h_{av} = \frac{1}{N^2} \sum_{i,j} h\left(x_i, y_j\right). \tag{4.1}$$

The difference $\overline{h} - h_{av}$, although small, is not zero and is a random function of the scan position on the plate [102]. This difference becomes larger the smaller the scan size is. Keeping in mind this point, which can be important in some situations, we can consider Eq. (4.1) as an approximate definition of the mean plane position.

An important characteristic of a rough surface is the rms roughness w, which is given as

$$w = \frac{1}{N^2} \sum_{i,j} \left[h\left(x_i, y_j\right) - h_{av}\right]^2. \tag{4.2}$$

It has the meaning of the surface width. More detailed information on the rough surface can be extracted from the height-difference correlation function defined for an infinite surface as

$$g(R) = \frac{1}{A} \int dxdy \ \ [h(\mathbf{r} + \mathbf{R}) - h(\mathbf{r})]^2, \tag{4.3}$$

where $\mathbf{r} = (x, y)$ and $\mathbf{R} = \mathbf{r}' - \mathbf{r}$.

A wide variety of surfaces, as for example, deposited thin films far from equilibrium, exhibit the so called self-affine roughness which is characterized besides the rms roughness amplitude w by the lateral correlation length ξ (indicating the average lateral feature size), and the roughness exponent $0 < H < 1$ [103–105]. Small values of $H \sim 0$ corresponds to jagged surfaces, while large values of $H \sim 1$ to a smooth hill valley morphology. For a special case of the self-affine rough surfaces $g(R)$ scales as

$$g(R) = \begin{cases} R^{2H}, & R \ll \xi, \\ 2w^2, & R \gg \xi. \end{cases} \tag{4.4}$$

The parameters w, ξ and H can be determined from the measured height-difference correlation function $g(R)$. This function can be extracted approximately from the AFM scans of the surface. An example is shown in Fig. 14. The top image is an AFM scan of 100 nm thick Au film. The bottom image shows the correlation function extracted from the image and its approximation with Eq. (4.4). From Eq. (4.2) it is found that $w \approx 1.5$ and from the power-law behavior of the correlation function it is found that $\xi \approx 22.4$ and $H \approx 0.9$. The latter value shows that deposited gold is described by smooth hills and valleys.

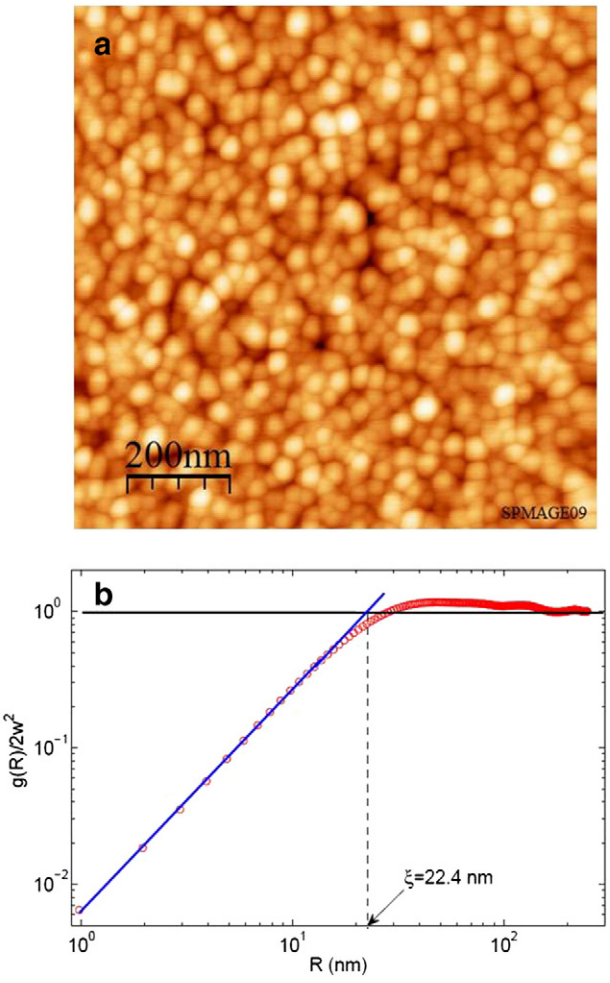

Fig. 14. (a) AFM image of a deposited gold film 100 nm thick. The image size is 1×1 μm^2. (b) The correlation function extracted from the image (red circles). Blue solid line is the linear fit (on log–log scale) that allows determination of both parameters ξ and H.

To find roughness correction to the force one has to know (see Section 4.2) the spectral density $\sigma(k)$ of the height–height correlation function $C(R)$. The latter is related to $g(R)$ as $g(R) = 2w^2 - C(R)$. An analytic form of the spectral density for a self-affine surface is given by [106]:

$$\sigma(k) = \frac{CHw^2\xi^2}{\left(1 + k^2\xi^2\right)^{1+H}}, \quad C = \frac{2}{1 - \left(1 + k_c^2\xi^2\right)^{-H}}. \tag{4.5}$$

Here C is a normalization constant [105,106] and $k_c = 2\pi/L_c$ is the cutoff wavenumber.

4.1.2. Distance upon contact and height distribution

The absolute distance separating two bodies is a parameter of principal importance for determination of the dispersion forces. In fact, when the bodies are brought into gentle contact they are still separated by some distance d_0, which we call the distance upon contact due to surface roughness. This parameter has a special significance for weak adhesion, which is mainly due to van der Waals forces across an extensive noncontact area [17]. In the modern precise measurements of the dispersion forces [8,94,95] d_0 is the main source of errors. The distance

upon contact is usually considerably larger than the rms roughness because it is defined by the highest asperities. It is important to clearly understand the origin of d_0, its dependence on the lateral size L of involved surfaces, and possible uncertainties in its value [107].

Consider two parallel rough plates facing each other. Each surface can be described by the roughness profile $h_i(x, y)$ ($i = 1, 2$ for plates 1 or 2) as shown in Fig. 15a. The averaged value over a large area is assumed to be zero $\langle h_i(x, y)\rangle = 0$. Then the local distance between the plates is

$$d(x, y) = d - h_1(x, y) - h_2(x, y). \tag{4.6}$$

This distance depends on the combined rough profile $h(x, y) = h_1(x, y) + h_2(x, y)$. Indeed, the averaged local distance has to give $\langle d(x, y)\rangle = d$. We can define the distance upon contact d_0 as the largest distance $d = d_0$, for which $d(x, y)$ becomes zero.

It is well known from contact mechanics [108] that the contact of two elastic rough plates is equivalent to the contact of a rough hard plate and an elastic flat plate with an effective Young's modulus E and a Poisson ratio ν. Here we analyze the contact in the limit of zero load when both bodies can be considered as hard. Then we can consider an equivalent configuration of a flat plate facing a rough plate with the roughness given by the combined profile $h(x, y)$ as shown in Fig. 15b. In this configuration d_0 is defined as the maximal peak of the combined profile.

Consider a combined image with the size L. It is assumed that this size is much larger than the correlation length ξ presenting typical feature size in the image. It means that the image area can be divided into a large number $N^2 = L^2/\xi^2$ of cells. The height of each cell (asperity) can be considered as a random variable h. The probability to find h smaller than some value z can be presented in a general form

$$P(z) = 1 - e^{-\phi(z)}, \tag{4.7}$$

where the "phase" $\phi(z)$ is a nonnegative and nondecreasing function of z. Note that Eq. (4.7) is just a convenient way to represent the data: instead of the cumulative distributions $P(z)$ we are using the "phase" $\phi(z)$, which carries more information about the tails of the distribution.

For a given asperity the probability to find its height above d_0 is $1 - P(d_0)$, then within the area of nominal contact one asperity will be higher than d_0 if

$$e^{-\phi(d_0)}\left(L^2/\xi^2\right) = 1 \quad \text{or} \quad \phi(d_0) = ln\left(L^2/\xi^2\right). \tag{4.8}$$

This condition can be considered as an equation for the height of the height asperity due to a sharp exponential behavior of the distribution tail. To solve Eq. (4.8) we have to know the function $\phi(z)$, which can be found from the roughness topography.

The cumulative distribution $P(z)$ can be extracted from combined images by counting pixels with the height below z. The probability density function $f(z)$ can be expressed as $f(z) = dP/dz$. The "phase" is calculated as $\phi(z) = -\ln(1 - P)$. The results are presented in Fig. 16b. The procedure of solving Eq. (4.8) is shown schematically by thin dashed lines, and the solution itself is the red solid curve in Fig. 16a. The blue dots with the error bars show the values of d_0 determined directly from the combined AFM images taken on different scales L. The error bars demonstrate variation of d_0 determined from different local areas of the size L^2 of homogeneous gold films [107]. Note that d_0 is considerably larger than w for all the scales $L \gg \xi$.

It has to be mentioned that the normal distribution fails to describe the data for Au films at large z. Other known distributions cannot satisfactory describe the data for all z. Asymptotically at large $|z|$ the data can be reasonably well fit with the generalized extreme value Gumbel distributions (green lines in Fig. 16b) [109]:

$$ln\,\phi(z) = \begin{cases} -\alpha z, & z \to -\infty \\ \beta z, & z \to \infty \end{cases} \tag{4.9}$$

It has to be stressed that the extreme value statistics describes quite well the tails of the distribution of all gold films investigated in [107].

4.2. Perturbative correction to the force

Suppose that the force per unit area between two flat plates is $F(d)$. If the rms roughness w of the combined profile $h(x, y)$ is small, $w \ll d$, but

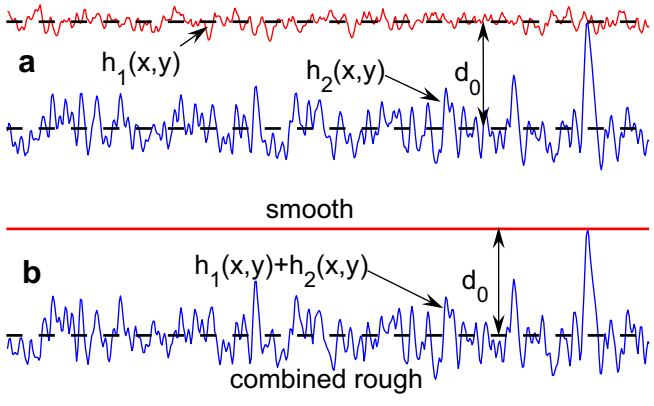

Fig. 15. Contact of two rough surfaces. (a) Two rough plates in contact. Roughness of each plate, $h_i(x, y)$, is counted from the mean plane shown by the dashed lines. The distance between bodies is the distance between these mean planes. (b) The interaction between two rough plates is equivalent to the interaction between a smooth plate and a rough plate with the roughness given by the combined profile $h(x, y)$. The distance upon contact, d_0, is the maximal peak within a given area.

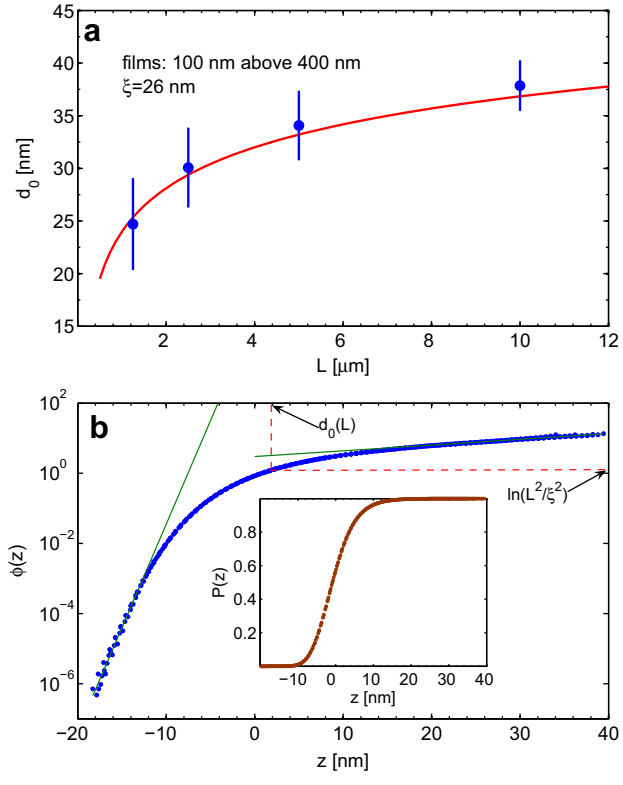

Fig. 16. (a) Distance upon contact as a function of the length scale. Dots with the error bars are the values calculated from the AFM images. The solid curve is the theoretical expectation according to Eq. (4.8). (b) Statistics of the surface roughness. Four 10×10 μm^2 images were used. The main graph shows the "phase" as a function of z. The green solid lines show the best fits at large positive and negative z. The red dashed lines demonstrate the solution of Eq. (4.8). The inset shows the cumulative distribution $P(z)$.

the correlation length is large, $\xi \gg d$, we can use the proximity force approximation and calculate the roughness correction additively. Averaging the force for local distances $d(x, y)$ and expanding it in power series in w/d one can present the energy between rough plates as

$$\mathcal{F}(d) = \langle F(d(x,y))\rangle \approx F(d) + \frac{F''}{2}\left\langle h^2 \right\rangle, \tag{4.10}$$

where $\langle h^2\rangle = w^2 = w_1^2 + w_2^2$ is the square of the combined rms roughness and $\mathcal{F}$ is the force between two rough plates. Eq. (4.10) defines the PFA roughness correction $\delta\mathcal{F}(d) = F''(d)w^2/2$. This correction was used in all early studies to estimate the roughness effect.

Genet et al. [23] noted that in most experimental configurations the condition $\xi \gg d$ is broken and PFA cannot be applied. In Refs. [24,25] a theory was developed, which is not restricted by the condition $\xi \gg d$. Within this theory the roughness correction is expressed via the spectral density of the rough surface $\sigma(k)$ as

$$\delta\mathcal{F}(d) = \int \frac{d^2k}{(2\pi)^2}\rho(k,d)\sigma(k), \tag{4.11}$$

where $\rho(k, d)$ is the roughness response function derived in [25]. This function is quite complicated and we do not provide it here refereeing to the original paper. The PFA result (4.10) is recovered from Eq. (4.11) in the limit of small wavenumbers $k \to 0$ when $\rho(k, d) \to F''(d)/2$. The roughness power spectrum is normalized by the condition $\int d^2k\sigma(k)/(2\pi)^2 = w^2$. The spectrum itself can be obtained from AFM scans and in the case of self-affine rough surfaces is given by Eq. (4.5).

Let us enumerate the conditions at which the PFA result given by Eq. (4.10) is valid. (i) The lateral dimensions of the roughness ξ must be much smaller than the system size L, $\xi \ll L$. This is usually the case in experiments. (ii) The rms roughness w must be small compared to the separation distance, $w \ll d$. This condition means that roughness is treated as perturbative effect. (iii) The lateral roughness dimensions must be much larger than the vertical dimensions, $w \ll \xi$ [25]. The last two assumptions are not always satisfied in the experiment.

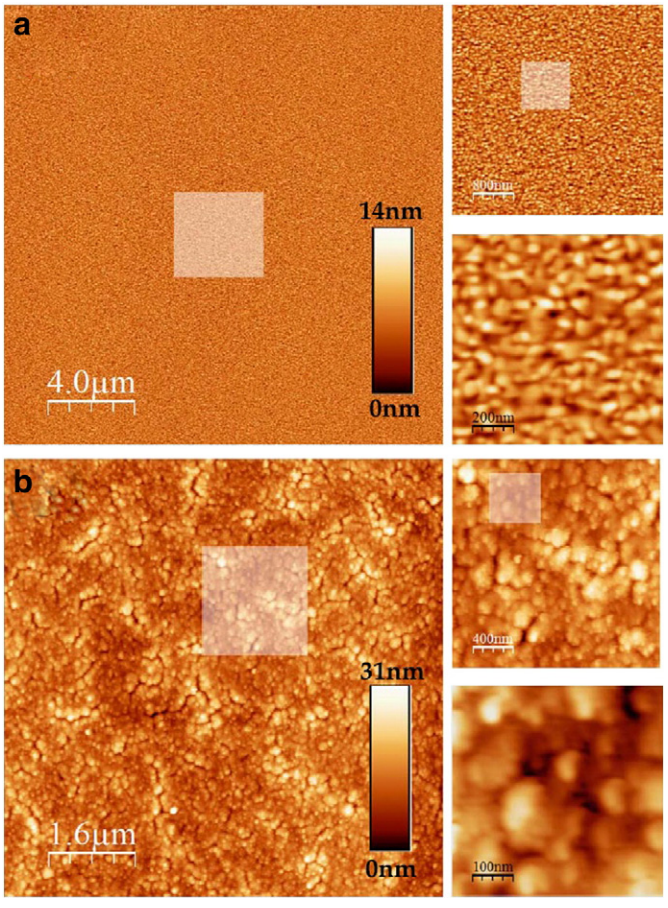

Fig. 17. AFM megascan of the 100 nm film (a) and the sphere (b). The insets show the highlighted areas at higher magnifications.

In the plate–plate configuration the force per unit area can be calculated as $\mathcal{F}(d)$. For the sphere–plate configuration, which is used in most of the experiments, the force is calculated with the help of PFA as $\mathcal{F}_{sp}(d) = 2\pi R\int_d^\infty \mathcal{F}(t)dt$. In contrast with the roughness correction the latter relation is justified for $d \ll R$, which holds true for most of the experimental configurations. We use the sphere–plate configuration to illustrate the roughness effect. The deposited gold films can be considered as self-affine. The perturbative correction to the Casimir force was calculated for the sphere–plate geometry [26,27,110] using the smoothest spheres with the parameters $w = 1.8$, $\xi = 22$, and $H = 0.9$ [111]. The plate roughness was different in dependence on thickness of the deposited Au films. We use the optical data for gold films measured in [112]. It was found that the PFA limit is quickly recovered for increasing correlation length. Deviations from PFA prediction for real films were found to be about 1–5% in the range of distances $d = 50 - 200$.

Therefore, for real rough surfaces the scattering theory gives a few percent correction to the force compared to the PFA. This difference is difficult to measure. However, at small separations both PFA and perturbation theory fail since the rms roughness becomes comparable in size to the separation distance. It is important to calculate the roughness effect when d is comparable with w. At the moment there is no a theoretical instrument to estimate the effect except a direct numerical analysis similar to that used in [113] (see also [22] as a review of the method). It would be interesting to do a full numerical analysis for rough films in close proximity when the perturbation theory does not work. However, even this approach seems quite complicated for real rough surfaces. On the other hand, it is experimentally possible to go to sufficiently small distances as was discussed in Section 3. A class of problems that can be solved using a relatively simple semi-analytical approach is presented in the next section.

4.3. Beyond perturbation theory

Here we are going to present an approach that allows us to calculate the roughness correction beyond perturbation theory. The approach is based on the experimental fact that the contact of rough bodies happens at the distance d_0, which is considerably larger than the rms roughness w. The distance upon contact depends on the lateral scale L but for $L > 1$ μm it is typically $d_0 > 3w$. This fact was established for gold films in many papers [26,58,93–95,96], where the Casimir force was measured, and checked directly by analysis of the AFM images [107]. However, at the moment there are no data for other materials and restrictions of the method are not clear yet.

The general idea of the method is very simple [27]. If two bodies are gently touched they are still separated by the distance d_0. If the area of nominal contact includes many asperities, the real contact happens only in one or a few highest asperities. The contribution of these highest peaks to the force has to be calculated precisely. It is possible to do because the distance between high peaks is large. Normal asperities with the height ~ w can still be calculated using the perturbation theory. Let us consider now the details of the approach.

4.3.1. Roughness statistics of Au films

A detailed analysis of the roughness statistics of different gold films was performed by van Zwol et al. [107]. The films were already described in Section 3.4. These films were optically characterized [112] in a wide frequency range from $0.03 < \omega < 9$ eV and were used to measure the roughness contribution to the dispersion forces [26]. The AFM images of the films presented in Fig. 12 cannot be used to extract

detailed information on the film roughness. This is because the scan size $L = 0.5$ μm is too small to draw conclusions on the statistics from one image. Practically it means that one has to analyze a large number of images to get reliable data but even this is difficult because the film is not absolutely homogeneous: images taken from different local places can poor correlate.

This practical problem was resolved [107] by collecting the so-called megascans for each film. These are high resolution AFM scans with the size up to 40×40 μm^2 and a lateral resolution of 4096×4096 pixels. The maximal area that was possible to scan on the sphere was 8×8 μm^2 (2048×2048 pixels). All images were flattened with linear filtering; for the sphere the parabolic filtering was used to exclude the effect of curvature. The images of 100 nm film and the sphere are shown in Fig. 17(a) and (b), respectively. Each image can be zoomed a few times due to high resolution. The detailed statistics is collected just from one image. In this way we can be sure that nonhomogeneity of the film plays a minimal role.

From all the images the cumulative distribution $P(z)$ was determined. Using this distribution the "phase" $\phi(z)$ has been calculated according to Eq. (4.7) and the probability density function was calculated as $f(z) = dP/dz$. In Fig. 18 the result is presented for the image of the roughest 1600 nm thick Au film. As was already mentioned the logarithm of the "phase" at large positive and negative z is well described by the linear behavior that is a signature of the extreme value statistics. Strong deviation of the tails from the normal distribution is well visible in the inset. The real film has much more high peaks than predicted by the normal distribution of the asperity heights. The latter is important to calculate the roughness effect beyond perturbation theory.

4.3.2. Roughness contribution

We can imagine a rough surface as a large number of asperities with the height ~ w and lateral size ξ, and occasional high peaks and deep pits. These peaks are high in the sense that their height is considerably larger than w, say > $3w$. The situation can be visualized as a lawn covered with grass and occasional high trees standing here and there. For this reason the model described in this subsection sometimes is called "lawn and threes" model.

The interacting surfaces are separated by the distance $d > d_0 > 3w$. Normal asperities with the height ~ w can be treated perturbatively because even at contact $(w/d)^2 \ll 1$ and the perturbation theory can be applied. For the high peaks the local distance between the bodies becomes small and the perturbation theory fails. Because the high peaks

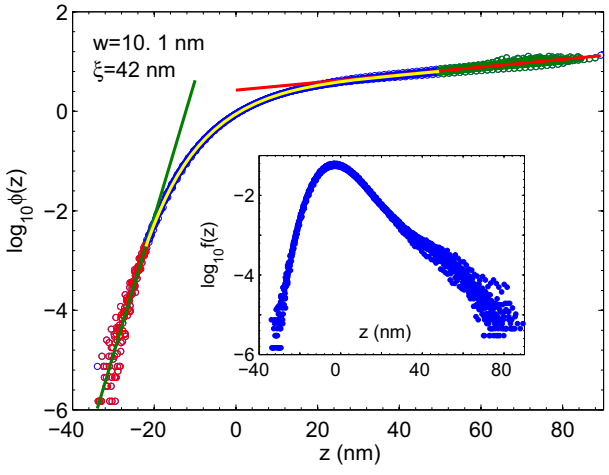

Fig. 18. The "phase" as a function of z for a 1600 nm gold film. The circles are the actual data extracted from the AFM image via $P(z)$. At large positive and large negative heights $log_{10}\phi(z)$ is well fitted by linear functions of z as it is shown by the straight lines. The curved line is a polynomial fit at intermediate z. The inset shows the probability density function $f(z)$. It demonstrates a significant deviation from the normal distribution.

are rare the average distance between them l is large. If $l \gg d$ then we can calculate the contribution of the high peaks independently on each other. Interaction of one high peak with a flat surface can be taken into account precisely using developed numerical or sometimes analytical methods [22].

The number of asperities N with a height $d_1 > 3w$ and lateral size ξ on the area L^2 is given by the equation similar to Eq. (4.8):

$$N = \frac{L^2}{\xi^2} e^{-\phi(d_1)}. \tag{4.12}$$

The average distance between these peaks is

$$l = \frac{L}{\sqrt{N}} = \xi e^{\phi(d_1)/2}. \tag{4.13}$$

One can choose the parameter d_1 in such a way that $l \gg d$. Its actual value lies in the interval $3w < d_1 < d_0$. If it happens that $d_1 > d_0$ than the perturbation theory can be applied for all asperities and there is no need to separate high asperities.

Suppose for a moment that the PFA can be applied to any roughness topography. Then the force between rough surfaces can be calculated as

$$\mathcal{F}(d) = \int_{d_1}^{d_0} \ldots + \int_{-d_0'}^{-d_1'} \ldots + \int_{-d_1'}^{d_1} dz f(z) F(d-z), \tag{4.14}$$

where $F(d)$ is the force between flat surfaces, $f(z) = dP/dz$ is the probability density function determined from the images of rough surfaces. The first integral is the contribution of high peaks, the second one accounts for the deep pits with the corresponding parameters d_1' and d_0', and the last term is the contribution of normal roughness.

We know that application of PFA to normal asperities is wrong but it is possible to apply the perturbation theory to the last term that has to be generalized as (only the roughness correction)

$$\delta\mathcal{F}_{PT}(d) = \frac{F''(d)}{2!} \int \frac{d^2k}{(2\pi)^2} \rho(k,d)\sigma(k). \tag{4.15}$$

Here $\sigma(k)$ is the Fourier spectrum of the roughness measured or calculated according to Eq. (4.5). The function $\rho(k, d)$ measures the deviation from the PFA and it is the same function introduced in Eq. (4.10). One can use for $\rho(k, d)$ the expressions found in [24,25].

The second term in Eq. (4.14) can be neglected because the force for deep pits is small and their number is not large. On the contrary, the first term in Eq. (4.14) is important and the PFA is applicable to this term because the high peaks do not influence each other. The final result for the force between rough surfaces can be written as

$$\mathcal{F}(d) = F(d) + \delta\mathcal{F}_{PT}(d) + \delta\mathcal{F}_{PFA}(d), \tag{4.16}$$

where $\delta\mathcal{F}_{PFA}$ is the contribution of the high peaks given by the relation

$$\delta\mathcal{F}_{PFA}(d) = \int_{d_1}^{d_0} dz f(z) \times \left[F(d-z) - F(d) + F'(d)z - \frac{F''}{2!}z^2\right]. \tag{4.17}$$

There last three terms in the square brackets exclude the contribution that was already included in $\delta\mathcal{F}_{PT}(d)$. Eqs. (4.16) and (4.17) give us the possibility to calculate the effect of roughness beyond the perturbation theory.

4.3.3. Comparison with the experiments

We have seen already in Sections 3.2 and 3.4 that the experiments demonstrate significant deviation of the roughness contribution to the force (or adhesion energy) from expectations. The described above

model that is going beyond the perturbation theory has a chance to settle the contradiction. It is difficult to make predictions for the experiment [17], where the adhesion energy between oxidized polysilicon surfaces was measured. This is because the detailed roughness of polysilicon surfaces was not collected. On the other hand, all the necessary information for the experiment [26] is available. In this experiment very strong deviation from the expected scaling of the force with distance was found. This is an optimal situation to check a new model. It was done for the first time by Broer et al. [27].

Gold films can be considered as self-affine. The spectral density of roughness for such films is given by Eq. (4.5) with the parameters w, ξ, and H determined directly from the images. The dielectric functions of the films needed for calculations were measured in [112]. This functions were used to evaluate the first term in Eq. (4.16) that is given by the Lifshitz formula (Eq. (2.25) for the sphere–plate configuration) and the function $\rho(k, d)$ needed for the second term. The last term responsible for the contribution of the high peaks is given by Eq. (4.17). This is the term that has to be responsible for the strong change of the force scaling. The probability density $f(z)$ is extracted from the AFM images of the films. In the simplest approach it is assumed that the force $F(d)$ entering under the integral in Eq. (4.17) is also given by Eq. (2.25). This assumption means that the high asperities are presented as pillars with the cross section $\xi \times \xi$ and a flat cap.

This assumption is justified by the following consideration. A few high peaks can give significant contribution if the local distance between the peak and the opposing surface is very small. The actual condition is $d - d_0 \ll \xi$. If this condition is true, then the shape of the pillar cap is not very important. It becomes important if $d - d_0 \sim \xi$ but in this case the contribution of high peaks to the force is small.

The result of calculations and the experimental data from [26] are shown in Fig. 19 for the roughest film 1600 nm, but similar situation is observed for the films 800 nm and 1200 nm thick. It is obvious that the model is able to explain the behavior of the force at small separations. This is due to the contribution of high peaks as the inset demonstrates (curve 2). It increases very sharp with the distance. On the other hand, the contribution of normal asperities is never large as the curve 3 shows.

If one would naively apply the additivity to calculate the effect of roughness in the dispersion forces (we call the approach "naive PFA"), the result would correspond to the dashed line in Fig. 19. For this naive PFA the force is given by the expression similar to Eq. (4.14)

$$\mathcal{F}(d) = \int_{-d_0'}^{d_0} dz f(z) F(d-z). \tag{4.18}$$

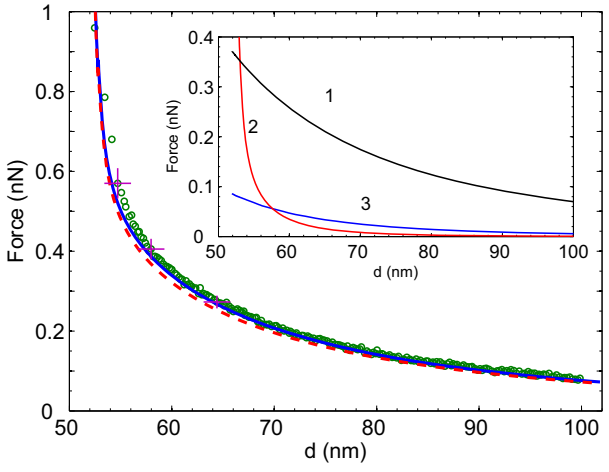

Fig. 19. The force between a Au-covered sphere (R = 50 μm) and a plate (1600 nm thick Au). The circles (green) are the experimental data. The vertical and horizontal bars show the experimental errors for a few points. The solid (blue) line is the result of the model. Naive application of the PFA to the force between rough bodies is shown by the dashed (red) curve. The inset shows different contributions to the force. 1 (black) is the force $F(d)$ between smooth surfaces. 2 (red) is the contribution of the high peaks. 3 (blue) is the perturbation theory correction. The sum of all three curves gives the solid line in the main panel.

At small distances this curve coincides with the exact model because the contribution of normal asperities is small but high asperities can be included additively. At larger distances there is some deviations between the curves but it is not large. This deviation is due to the perturbation theory contribution (4.15), which never dominates. One can conclude that the reason for a strong deviation of the force from normal scaling is found and this reason is a large contribution of high asperities which locally approach the opposite surface very closely.

Influence of the shape of high peaks on the force was analyzed in detail [110] in spite of the arguments above that it should not be significant. One has to note that the shape cannot be determined from AFM scans because the tip radius is comparable with the curvature radius of a peak. The following model shapes were considered: a rectangular pillar with a flat or spherical cap, an ellipsoid with half-axes d_0 and $\xi/2$, and a cone with height d_0 and bottom diameter ξ. For a flat pillar the force between a peak and a flat surface was calculated with the Lifshitz formula (2.19). For a pillar with a spherical cap the force was evaluated using sphere–plate interaction that does not assume applicability of PFA [114]. For an ellipsoid and cone the force was calculated numerically with a finite-difference time-domain (FDTD) [115] program called Meep [116]. It was found that the all possible shapes of peaks are nearly equivalent except of the cone. The conical shape predicts the force to be too small to explain the experiment. One could expect it because the tip of the cone gives very small contribution to the force (small area). Due to the shape the force variation is smaller than 5% nearby the contact.

4.4. What we learned from the theory

In general roughness contribution to the dispersion forces is a complicated problem when the distance between interacting bodies become comparable with the rms roughness, $d \sim w$. The difficulty is related to the nonadditivity of the dispersion forces. Similar problem appears for the electrostatic interaction between rough bodies.

Naive PFA approach neglects the nonadditivity problem. The force is calculated as the sum of independent forces between small parallel patches. For randomly rough surfaces the force together with the roughness contribution is given by Eq. (4.18). To use this expression one has to know the very detailed information about the probability density function. The tails of the distribution are especially important. The probability density can be extracted from AFM images of the interacting surfaces. The probability to find a high peak on the rough surface is very important because the high peaks can approach locally close to the opposite surface and give large contribution to the force. A strong disadvantage of the naive PFA approach is that the precision of this method cannot be controlled. It is a good approximation if the correlation length is much larger than the distance between bodies, $\xi \gg d$. Nevertheless, in many situations the approximation works well even if this condition is broken.

At large distances, $d \gg w$, the roughness effect can be treated perturbatively. A method to calculate the roughness correction in this situation was developed [24]. It is based on the scattering theory and it can be applied even if the condition $\xi \gg d$ is not fulfilled. One has to know the roughness power spectrum that can be determined from AFM images of the interacting surfaces. In this situation the roughness correction is treated as a small correction to the Lifshitz formula that describes the main contribution to the force. This correction is given by Eq. (4.15).

When the surfaces are close to contact the perturbative correction does not describe the situation as was demonstrated experimentally

[17,26]. However, the ratio $(w/d)^2$ stays small even at contact because the minimal distance between bodies is $d_0 > 3w$ and one would expect that the perturbation theory is applicable. The explanation of the puzzle was given for gold films where the problem is clearly observed [26]. Careful analysis of these films [107] revealed significant deviations from the normal distribution. The number of high peaks for gold films was much larger than predicted by the normal distribution. This property gave an idea for the "lawn and trees" model [27]. In this model asperities with normal height ~ w are treated perturbatively, while contribution of high asperities > $3w$ can be calculated precisely. Because the distance between high asperities is large they do not influence each other and they can be treated additively. This approach successfully explained the experimental data. It also gives a hint why the proximity force approximation works better than it is expected: at small separations high peaks play more important role than normal asperities, but for these peaks the PFA can be applied.

5. Conclusions

The main purpose of this paper is to analyze the influence of natural roughness on the dispersion interaction of two closely separated bodies. We did not discuss in detail loaded contact when elastic or plastic deformations of some asperities takes place (for recent analysis see [117]). A convenient way to investigate influence of roughness on the dispersion forces is analysis of contactless interaction between bodies approaching the contact between highest asperities.

The problem considered here is important for a wide range of applications where one has to tune forces acting in air or in liquid environment between components of different micro or nanodevices. These devices have areas large enough but gap small enough for these forces to draw components together and even lock them permanently. Roughness also influences adhesion, friction, wetting, and stiction.

For non-experts in the dispersion forces we gave the introduction of the forces between flat and gently curved surfaces. Special attention is paid on the physical understanding of common origin of such forces as van der Waals, Casimir, and Casimir–Lifshitz. The physical basis of the Lifshitz theory [4] was briefly presented. This theory explains the dispersion forces as interaction between bodies due to electromagnetic field induced by current fluctuations in the bodies. We provided a number of helpful relations to use in different practical situations.

There are many experiments where the effect of roughness was important but only in a few critical experiments this effect was investigated in detail. We reviewed these experiments in Chapter 3. Nonadditivity of the dispersion forces was proven experimentally using the interaction between corrugated plates and a sphere [56]. The fact of nonadditivity is a serious obstacle in the development of the theory. After careful investigation of the stiction problem that results in malfunction of many microelectromechanical devices it becomes clear that it is possible to exclude strong adhesion forces like capillary of chemical forces, but it is not possible to switch off the dispersion interaction. Special investigation of adhesion due to this interaction revealed the significant role of roughness [17]. The effect of roughness happened to be considerably stronger than one would expect for interaction between flat surfaces.

Influence of roughness was investigated also using the surface force apparatus. This method is better designed for investigation of strong adhesion. It was demonstrated that attractive dispersion forces depend on the details of the height distribution of the nano-scale asperities [85]. The forces measured with atomic force microscope or with torsional oscillator also showed the dependence on roughness. However, in most cases it was done at rather large distances when the roughness effect is small. Only in one experiment influence of roughness was investigated specifically at the smallest possible distance between sphere and plate covered with deposited gold. In this experiment it was demonstrated that roughness changed significantly the expected scaling of the force with the distance [26]. Moreover, it seemed that the observed effect cannot be explained by any existed theory until recently.

The state of the theory was reviewed is Chapter IV. First, we described the ways to characterize a rough surface with emphasis on the minimal distance between bodies. This distance d_0 is an important parameter for interaction at smallest separations. For gold films d_0 is considerably larger than rms roughness, $d_0 = (3-5)w$, depending on the size of the interaction area [107]. The roughness correction to the force can be expressed explicitly if the distance between bodies is much larger than the rms roughness, $d \gg w$. In this case one can apply the perturbation theory using as a small parameter the ratio w/d. As input data one has to know also the spectral density of the rough surface. For a smooth roughness profile, when the correlation length ξ is large, $\xi \gg d$, it is possible to use additivity and the correction can be easily found. In the opposite situation, which is quite often the case, one has to use a complicated approach based on the scattering theory. Nevertheless, the explicit result for the correction exists [24].

Experiments demonstrate that significant deviations from theoretical expectations are observed for the parameter $(w/d)^2 \sim 0.01$ where the perturbation theory has to work fine. To understand this phenomena careful analysis of the roughness statistics was undertaken for deposited gold films. It was found that the probability to find a high peak is considerably higher than it is expected from the normal distribution [107]. High peaks and deep pits for gold films are described much better with the extreme value statistics. Despite that only a small area is covered with high peaks, they can be important because these peaks locally can approach very close to the opposing surface. Using these observations the so-called "lawn and trees" model was proposed [27] to calculate the force close to contact. In this model normal asperities ($\sim w$) are treated perturbatively, while the contribution of high asperities is calculated precisely. The latter is possible because the distance between high peaks is large and they can be taken into account additively. This model reproduced successfully the experimental data for rough gold films. It also explained why the naive approach based on the proximity force approximation (additivity) often works better than it is expected.

Serious investigation of roughness on the dispersion forces has started relatively recently. Many questions are still open. Here we would like to enumerate some important problems that have to be analyzed. Few experiments characterize the influence of roughness on the dispersion forces in liquid environment. The surface force apparatus is able to give valuable information but it is better designed for very small separations and flat surfaces. AFM experiments in dielectric liquids and electrolytes could fill this gap. There was no special attention to roughness contributions in the existing AFM experiments in liquids.

It was demonstrated that the "lawn and trees" model was able to reproduce the experimental data for gold films. How general the model is? At this moment it is difficult to answer the question because careful investigation of the roughness of different materials is needed. It has to be stressed that a few AFM images with the size ~ 1 μm are not sufficient to collect the data on roughness. Different materials especially those used in microtechnology have to be carefully characterized. It is clear that there is a class of materials that has roughness similar to that of gold. It is obvious also that some materials cannot be described in this way, for example, materials with terraces. Is it possible to explain roughness effect for some intermediate situations? If roughness can be described by the normal distribution, still real contact happens at high peaks. Will the model work in this case?

In any case evaluation of the roughness contribution seems not possible in the situation when the distance is comparable with the rms roughness, $w \sim d$. The only possible approach here is numerical. This approach has been developed very successfully [22]. It was applied to calculate the force between many geometrical configurations but the roughness effect never has been tackled. These calculations combined with careful characterization of the surfaces and model predictions could give solid ground for the roughness problem.

Acknowledgments

VBS is grateful to L. B. Boinovich for the idea to write this review. Both authors thank P. van Zwol and W. Broer for their collaboration in experimental and theoretical aspects of the roughness effect. GP acknowledges support from Zernike Institute for Advanced Materials and Material Innovation Institute M2i (project MC3.05242). The authors benefited from the exchange of ideas within the ESF Research Network CASIMIR.

References

[1] London F. Z Phys 1930;63:245.
[2] Casimir HBG. Proc K Ned Akad Wet 1948;51:793.
[3] Lifshitz EM. Zh Eksp Teor Fiz 1955;29:894 [Soviet Phys. JETP 2, 73 (1956)].
[4] Dzyaloshinskii ID, Lifshitz EM, Pitaevskii LP. Usp Fiziol Nauk 1961;73:381 [Soviet Phys. Usp. 4, 153 (1961)].
[5] Serry FM, Walliser D, Maclay GJ. J Microelectromech Syst 1995;4:193.
[6] Serry FM, Walliser D, Maclay GJ. J Appl Phys 1998;84:2501.
[7] Buks E, Roukes ML. Phys Rev B 2001;63:033402.
[8] Chan HB, Aksyuk VA, Kleiman RN, Bishop DJ, Capasso F. Phys Rev Lett 2001;87:211801.
[9] Derjaguin B, Landau L. Acta Physicochim URSS 1941;14:633 [republished in Prog. Surf. Sci. 43, 30 (1993)].
[10] Verwey EJW, Overbeek JTG. Theory of the stability of lyophobic colloids. Elsevier Publishing Company; 1948.
[11] Mahanty J, Ninham BW. Dispersion forces (colloid science). New York: Academic Press; 1977.
[12] Derjaguin BV, Churaev NV, Muller VM. Surface forces. New York: Consultant Bureau; 1987.
[13] Israelachvili JN. Intermolecular and surface forces. London: Academic Press; 1992.
[14] Parsegian VA. Van der Waals forces. Cambridge, UK: Cambridge University Press; 2006.
[15] Boinovich LB. Russ Chem Rev 2007;76:471.
[16] Maboudian R, Howe RT. J Vac Sci Technol B 1997;15:1.
[17] DelRio FW, de Boer MP, Knapp JA, Reedy Jr ED, Clews PJ, Dunn ML. Nat Mater 2005;4:629.
[18] Lifshitz EM, Pitaevskii LP. Statistical physics, part 2. Oxford: Pergamon; 1980.
[19] Casimir HBG, Polder D. Phys Rev 1948;73:360.
[20] Maia Neto PA, Lambrecht A, Reynaud S. Phys Rev A 2008;78:012115.
[21] Canaguier-Durand A, Maia Neto PA, Lambrecht A, Reynaud S. Phys Rev A 2010;82:012511.
[22] Rodriguez AW, Caspasso F, Johnson SG. Nat Photonics 2011;5:211.
[23] Genet C, Lambrecht A, Maia Neto P, Reynaud S. Europhys Lett 2003;62:484.
[24] Maia Neto P, Lambrecht A, Reynaud S. Europhys Lett 2005;69:924.
[25] Maia Neto P, Lambrecht A, Reynaud S. Phys Rev A 2005;72:012115.
[26] van Zwol PJ, Palasantzas G, De Hosson JTM. Phys Rev B 2008;77:075412.
[27] Broer W, Palasantzas G, Knoester J, Svetovoy VB. Europhys Lett 2011;95:30001.
[28] van der Waals JD. Over de Continueiteit van den Gas- en Vloeistoftoestand (thesis) ; 1873 [Leiden].
[29] Hamaker HC. Phisica 1937;4:1058.
[30] Hunter RJ. Foundations of colloid science. Oxford: Clarendon Press; 1987.
[31] de Boer JH. Trans Faraday Soc 1936;32:21.
[32] Rytov SM, Kravtsov YA, Tatarskii VI. Principles of statistical radiophysics. Elements of random fields, vol. 3. Berlin: Springer; 1989 [This is an enlarged edition of S. M. Rytov, Theory of Electric Fluctuations and Thermal Radiation (Academy of Sciences of USSR, Moscow, 1953) (in Russian)].
[33] Landau LD, Lifshitz EM. Electrodynamics of continuous media. Oxford: Pergamon Press; 1963.
[34] Reid MTH, Rodriguez AW, White J, Johnson SG. Phys Rev Lett 2009;103:040401.
[35] Callen HB, Welton TA. Phys Rev 1951;83:34.
[36] Agarwal GS. Phys Rev A 1975;11:230.
[37] Eckhardt W. Phys Rev A 1984;29:1991.
[38] Antezza M, Pitaevskii LP, Stringari S, Svetovoy VB. Phys Rev A 2008;77:022901.
[39] Landau LD, Lifshitz EM. Statistical physics, part 1. Oxford: Pergamon; 1986.
[40] Pitaevskii LP. Phys Rev A 2006;73:047801 [C. Raabe and D.-G. Welsch, Phys. Rev. A 73, 047802].
[41] Palasantzas G, Svetovoy VB, van Zwol PJ. Phys Rev B 2009;79:235434.
[42] Lambrecht A, Reynaud S. Eur Phys J D 2000;8:309.
[43] Zhou F, Spruch L. Phys Rev A 1995;52:297.
[44] Tomaš MS. Phys Rev A 2002;66:052103.
[45] Derjaguin BV. Kolloid Z 1934;69:155.
[46] Blocki J, Randrup J, Swiatecki WJ, Tsang CF. Ann Phys (NY) 1977;105:427.
[47] White LR. J Colloid Interface Sci 1983;95:286.
[48] Derjaguin BV, Abrikosova II, Lifshitz EM. Q Rev Chem Soc 1956;10:295.
[49] Brown-Hayes M, Dalvit DAR, Mazzitelli FD, Kim WJ, Onofrio R. Phys Rev A 2005;72:052102.
[50] Smythe WR. Static and dynamic electricity. New York: McGraw-Hill; 1968 78.
[51] Golestanian R, Kardar M. Phys Rev A 1998;58:1713.
[52] Emig T, Hanke A, Kardar M. Phys Rev Lett 2001;87:260402.
[53] Büscher R, Emig T. Phys Rev A 2004;69:062101.
[54] Roy A, Mohideen U. Phys Rev Lett 1999;82:4380.
[55] Klimchitskaya GL, Zanette SI, Caride AO. Phys Rev A 2000;63:014101.
[56] Chan HB, Bao Y, Zou J, Cirelli RA, Klemens F, Mansfield WM, et al. Phys Rev Lett 2008;101:030401.
[57] Chan HB, Bao Y, Zou J, Cirelli RA, Klemens F, Mansfield WM, et al. Int J Mod Phys A 2010;25:2212.
[58] Chan HB, Aksyuk VA, Kleiman RN, Bishop DJ, Capasso F. Science 2001;291:1941.
[59] Decca RS, López D, Fischbach E, Krause DE. Phys Rev Lett 2003;91:050402.
[60] Palik ED, editor. Handbook of optical constants of solids. New York: Academic Press; 1985.
[61] Bao Y, Guérout R, Lussange J, Lambrecht A, Cirelli RA, Klemens F, et al. Phys Rev Lett 2010;105:250402.
[62] Lambrecht A, Neto PAM, Reynaud S. New J Phys 2006;8:243.
[63] Rahi SJ, Emig T, Graham N, Jaffe RL, Kardar M. Phys Rev D 2009;80:085021.
[64] Intravaia F, Koev S, Jung IW, Talin AA, Davids PS, Decca RS, et al. Nat Commun 2013;4:2515.
[65] Intravaia F, Lambrecht A. Phys Rev Lett 2005;94:110404.
[66] Guckel H, Burns DW. Sensors Actuators 1989;20:117.
[67] Maboudian R. Surf Sci Rep 1998;30:207.
[68] Zhao YP, Wang LS, Yu TX. J Adhes Sci Technol 2003;17:519.
[69] de Boer MP, Michalske TA. J Appl Phys 1999;86:817.
[70] de Boer MP, Knapp JA, Michalske TA, Srinivasan U, Maboudian R. Acta Mater 2000;48:4531.
[71] Knapp JA, de Boer MP. J Microelectromech Syst 2002;11:754.
[72] Mastrangelo CH, Hsu CH. J Microelectromech Syst 1993;2:33.
[73] Mastrangelo CH, Hsu CH. J Microelectromech Syst 1993;2:44.
[74] Houston MR, Howe RT, Maboudian R. J Appl Phys 1997;81:3474.
[75] Maboudian R, Carraro C. Annu Rev Phys Chem 2004;55:35.
[76] Srinivasan U, Houston MR, Howe RT, Maboudian R. J Microelectromech Syst 1998;7:252.
[77] Kim BH, Chung TD, Oh CH, Chun K. J Microelectromech Syst 2001;10:33.
[78] Bens M, Rosenberg KJ, Kramer EJ, Israelachvili JN. J Phys Chem B 2006;110:11884.
[79] Chen NH, Maeda N, Tirrell M, Israelachvili J. Macromolecules 2005;38:3491.
[80] Fuller KNG, Tabor D. Proc R Soc Lond Ser A 1975;345:327.
[81] Persson BN. J Phys Rev Lett 2001;87:116101.
[82] Hyun S, Pei L, Molinari JF, Robbins MO. Phys Rev E 2004;70:026117.
[83] Zappone B, Rosenberg KJ, Israelachvili J. Tribol Lett 2007;26:191.
[84] Xia YN, Whitesides GM. Annu Rev Mater Sci 1998;28:153.
[85] Valtiner M, Kristiansen K, Greene GW, Israelachvili JN. Adv Mater 2011;23:2294.
[86] Israelachvili JN, McGuiggan PM. Science 1988;241:795.
[87] Bhushan B, Israelachvili JN, Landman U. Nature 1995;374:607.
[88] Yoshizawa H, Chen YL, Israelachvili J. J Phys Chem 1993;97:4128.
[89] Frechette J, Vanderlick TK. Langmuir 2001;17:7620.
[90] Chai L, Klein J. Langmuir 2007;23:7777.
[91] Pashley RM, Israelachvili JN. J Colloid Interface Sci 1984;97:446.
[92] Mohideen U, Roy A. Phys Rev Lett 1998;81:4549.
[93] Iannuzzi D, Lisanti M, Capasso F. Proc Natl Acad Sci U S A 2004;101:4019.
[94] de Man S, Heeck K, Iannuzzi D. Phys Rev A 2009;79:024102.
[95] Harris BW, Chen F, Mohideen U. Phys Rev A 2000;62:052109.
[96] Decca RS, López D, Fischbach E, Klimchitskaya GL, Krause DE, Mostepanenko VM. Ann Phys (NY) 2005;318:37.
[97] van Zwol PJ, Palasantzas G, Th J, De Hosson M. Proc SPIE 2008;6800:68000E.
[98] Palasantzas G, Svetovoy VB, van Zwol PJ. Int J Mod Phys B 2010;24:6013.
[99] Munday JN, Capasso F. Phys Rev A 2007;75:060102(R).
[100] Munday JN, Capasso F, Parsegian VA, Bezrukov SM. Phys Rev A 2008;78:032109.
[101] Munday JN, Capasso F, Parsegian VA. Nature 2009;457:170.
[102] van Zwol PJ, Svetovoy VB, Palasantzas G. In: Dalvit D, Milonni P, Roberts D, da Rosa F, editors. Lecture notes in physics "Casimir physics". , Springer-Verlag; 2011. p. 311–43.
[103] Meakin P. Phys Rep 1993;235:189.
[104] Krim J, Palasantzas G. Int J Mod Phys B 1995;9:599.
[105] Zhao Y, Wang G-C, Lu T-M. Characterization of amorphous and crystalline rough surfaces—principles and applications. Academic Press; 2001.
[106] Palasantzas G. Phys Rev B 1993;48:14472 (49, 5785 (1994)).
[107] van Zwol PJ, Svetovoy VB, Palasantzas G. Phys Rev B 2009;80:235401.
[108] Greenwood JA, Williamson JBP. Proc R Soc A 1966;295:300.
[109] Coles S. An introduction to statistical modelling of extreme values. Berlin: Springer; 2001.
[110] Broer W, Palasantzas G, Knoester J, Svetovoy VB. Phys Rev B 2012;85:155410.
[111] van Zwol PJ, Palasantzas G, van de Schootbrugge M, Th J, De Hosson M. Appl Phys Lett 2008;92:054101.
[112] Svetovoy VB, van Zwol PJ, Palasantzas G, Th J, De Hosson M. Phys Rev B 2008;77:035439.
[113] Rodriguez A, Ibanescu M, Iannuzzi D, Capasso F, Joannopoulos JD, Johnson SG. Phys Rev Lett 2007;99:080401.
[114] Canaguier-Durand AM, Neto PA, Cavero-Pelaez I, Lambrecht A, Reynaud S. Phys Rev Lett 2009;102:230404.
[115] Taflove A, Hagness SC. Computational electrodynamics: the finite-difference time-domain method. London and Boston: Artech House; 2005.
[116] Oskooi AF, Roundy D, Ibanescu M, Bermel P, Joannopoulos JD, Johnson SG. Comput Phys Commun 2010;181:687.
[117] Parsons DF, Walsh RB, Craig VSJ. J Chem Phys 2014;140:164701.